

NASA/CR—2008-215216



Investigation of Flow Instabilities in the Inlet Ducts of DP-1C VTOL Aircraft

Jan Lepicovsky
ASRC Aerospace Corporation, Cleveland, Ohio

June 2008

NASA STI Program . . . in Profile

Since its founding, NASA has been dedicated to the advancement of aeronautics and space science. The NASA Scientific and Technical Information (STI) program plays a key part in helping NASA maintain this important role.

The NASA STI Program operates under the auspices of the Agency Chief Information Officer. It collects, organizes, provides for archiving, and disseminates NASA's STI. The NASA STI program provides access to the NASA Aeronautics and Space Database and its public interface, the NASA Technical Reports Server, thus providing one of the largest collections of aeronautical and space science STI in the world. Results are published in both non-NASA channels and by NASA in the NASA STI Report Series, which includes the following report types:

- **TECHNICAL PUBLICATION.** Reports of completed research or a major significant phase of research that present the results of NASA programs and include extensive data or theoretical analysis. Includes compilations of significant scientific and technical data and information deemed to be of continuing reference value. NASA counterpart of peer-reviewed formal professional papers but has less stringent limitations on manuscript length and extent of graphic presentations.
- **TECHNICAL MEMORANDUM.** Scientific and technical findings that are preliminary or of specialized interest, e.g., quick release reports, working papers, and bibliographies that contain minimal annotation. Does not contain extensive analysis.
- **CONTRACTOR REPORT.** Scientific and technical findings by NASA-sponsored contractors and grantees.
- **CONFERENCE PUBLICATION.** Collected

papers from scientific and technical conferences, symposia, seminars, or other meetings sponsored or cosponsored by NASA.

- **SPECIAL PUBLICATION.** Scientific, technical, or historical information from NASA programs, projects, and missions, often concerned with subjects having substantial public interest.
- **TECHNICAL TRANSLATION.** English-language translations of foreign scientific and technical material pertinent to NASA's mission.

Specialized services also include creating custom thesauri, building customized databases, organizing and publishing research results.

For more information about the NASA STI program, see the following:

- Access the NASA STI program home page at <http://www.sti.nasa.gov>
- E-mail your question via the Internet to help@sti.nasa.gov
- Fax your question to the NASA STI Help Desk at 301-621-0134
- Telephone the NASA STI Help Desk at 301-621-0390
- Write to:
NASA Center for AeroSpace Information (CASI)
7115 Standard Drive
Hanover, MD 21076-1320

NASA/CR—2008-215216



Investigation of Flow Instabilities in the Inlet Ducts of DP-1C VTOL Aircraft

Jan Lepicovsky
ASRC Aerospace Corporation, Cleveland, Ohio

Prepared under Grant NNCO6BA07B

National Aeronautics and
Space Administration

Glenn Research Center
Cleveland, Ohio 44135

June 2008

Acknowledgments

The work was performed under the ONR contract SAA3-675 managed by Mr. J.F. Kinzer, and NASA subcontract NNCO6BA07B managed by Mr. C.L. Meyers. The author would like to thank Mr. A.A. DuPont, president of DAC, and the entire DAC crew for extraordinary support and cooperation during these tests. Without their help it would be impossible to acquire data presented in a short test period of three days. The support of Mr. J.A. Burkhart of ASRC Aerospace Corporation is also gratefully acknowledged.

Trade names and trademarks are used in this report for identification only. Their usage does not constitute an official endorsement, either expressed or implied, by the National Aeronautics and Space Administration.

This work was sponsored by the Fundamental Aeronautics Program at the NASA Glenn Research Center.

Level of Review: This material has been technically reviewed by NASA technical management.

Available from

NASA Center for Aerospace Information
7115 Standard Drive
Hanover, MD 21076-1320

National Technical Information Service
5285 Port Royal Road
Springfield, VA 22161

Available electronically at <http://gltrs.grc.nasa.gov>

Investigation of Flow Instabilities in the Inlet Ducts of DP-1C VTOL Aircraft

Jan Lepicovsky
ASRC Aerospace Corporation
Cleveland, Ohio 44135

Abstract

An investigation of flow instabilities in the inlet ducts of a two-engine vertical takeoff and landing aircraft DP-1C is described in this report. Recent tests revealed that the engines stall during run ups while the aircraft is operating on the ground. These pop stalls occurred at relatively low power levels, sometimes as low as 60% of the engine full speed. Inability to run the engines up to the full speed level is attributed to in-ground effects associated with hot gas ingestion. Such pop stalls were never experienced when the aircraft was tested on an elevated grid platform, which ensured that the aircraft was operating in out-of-the-ground-effect conditions. Based on available information on problems experienced with other vertical takeoff and landing aircraft designs, it was assumed that the engine stalls were caused by partial ingestion of hot gases streaming forward from the main exit nozzle under the aircraft inlets, which are very close to the ground. It was also suggested that the nose wheel undercarriage, located between the inlets, may generate vortices or an unstable wake causing intense mixing of hot exit gases with incoming inlet flow, which would enhance the hot gas ingestion. After running a short three-day series of tests with fully instrumented engine inlets, it is now believed the most probable reason for engine pop stalls are random ingestions of a vortex generated between the two streams moving in opposite directions: outbound hot gas stream from the main nozzle close to the ground and inbound inlet flow above. Originally, the vortex is in a horizontal plane. However, at a certain velocity ratio of these two streams, the vortex attaches either to the ground or the aircraft surface at one end and the other end is swallowed by one of the aircraft inlets. Once the vortex enters the inlet duct, a puff of hot air can be sucked through the vortex core into the engine, which causes a serious inlet flow field distortion followed by an engine stall. Once the engine stalls, the outflow from the inlet pushes the vortex away and the engine resumes normal operation. This hypothesis needs to be verified experimentally; e.g., by extensive smoke flow visualization ahead of the aircraft inlets.

The report is divided into several chapters presenting background information, detailed description of modules for unsteady pressure measurements, data acquisition setup, and an instrumentation layout. This is followed by an overview of two basic test conditions, which are out-of-the-ground effect tests and in-the-ground effect tests. In the chapter on the in-the-ground effect tests, the experimental results for three aircraft configurations are presented. The aircraft configurations investigated were (1) deployed bare nose wheel tests, (2) deployed faired nose wheel tests, and (3) retracted nose wheel tests. In the final chapter of the report a summary of the in-the-ground effect tests is presented. Based on analysis of the results of all the tests performed it appears that the engine pop stalls are most likely evoked by a sudden ingestion of a vortex generated between two streams running in opposite directions; the hot jet exit stream running along the ground and the cold stream of air above being sucked into the aircraft inlets.

Nomenclature

List of symbols

α	[<i>deg, hr</i>]	port clockwise angular position
f	[<i>Hz, kHz</i>]	frequency
f_{LP}	[<i>Hz</i>]	low-pass filter cut-off frequency
m_A	[<i>kg.s⁻¹</i>]	actual mass flow rate
m_C	[<i>kg.s⁻¹</i>]	mass flow rate corrected for standard day conditions
NI	[<i>%</i>]	engine speed
p_{AMP}	[<i>Pa</i>]	amplitude of pressure oscillations
t	[<i>ms</i>]	time
V_A	[<i>m.s⁻¹</i>]	actual flow velocity at inlet lip during engine pop stall
V_0	[<i>m.s⁻¹</i>]	mean flow velocity at inlet lip
x	[<i>mm, in</i>]	port distance from fan front face
π_x	[<i>l</i>]	pressure ratio (relative to ambient pressure)

Abbreviations

BPF	blade passing frequency
IGE	in-ground effects
MCU	mobile control unit
OGE	out-of-the-ground effects
RSF	rotor shaft frequency
VTOL	vertical takeoff and landing

1 Background

Recent tests of the vertical takeoff and landing (VTOL) aircraft DP-1C revealed that the engines stall during run ups while the aircraft is operating on the ground (Ref. 1). These pop stalls occurred at relatively low power levels, sometimes as low as 60% of the engine full speed. Inability to run the engines up to the full speed level is attributed to in-ground effects (IGE) associated with hot gas ingestion. Such pop stalls were never experienced when the aircraft was tested on a 3.3 m (10 ft) high grid platform (Fig. 1-1) with the engines running up to the full design speed. The elevated platform ensures that the aircraft is operating in out-of-the-ground-effect (OGE) conditions.

Based on available information on IGE problems experienced with other VTOL aircraft designs, in particular the Bell X-14 aircraft (Ref. 2), it was assumed that the engine stalls were caused by partial ingestion of hot gases streaming forward from the main exit nozzle under the aircraft inlets, which are very close to the ground. It was also suggested that the nose wheel undercarriage, located between the inlets, may generate vortices or an unstable wake causing intense mixing of hot exit gases with incoming inlet flow, which would enhance the hot gas ingestion.

Hot gas ingestion problems of aircraft AV-8B were solved by redirecting the fountain flow away from the inlets deepening the side strakes and canting the fence

further forward (Ref. 3). In case of the airplane DP-1C, several attempts to prevent the hot flow lift up by inserting a 'roof' above the nose wheel did not prevent the engine stalls. Also a fence around the inlets (Fig. 1-2), which simulated a similar arrangement on the Bell X-14, did not succeed in elimination of engine stalls. Later on, laser-sheet flow visualization tests were carried out to map the flow around the engine inlets; however, no firm conclusion was reached about the cause of the engine stalls. A detailed description of these experiments is presented in Ref. 4.

After reviewing the results of these trials it was suggested that the engine stalls may be caused by either an inlet 'organ pipe' resonance excited by a vortex street generated by the nose wheel, or by inlet instability due to the mutual interaction of two closely coupled engine inlets (flow swinging). The latter option was based on apparent flow jumping between the inlets sometimes observed during the laser-sheet flow visualization. A third possibility was that the engine stalls are caused by a ground vortex being ingested into the engine inlet. Of course, the core of ingested ground vortex would also suck in hot gas from the exit nozzle stream adjacent to the ground.

In order to assess any of these three options, it was decided to run only one engine, while the other engine was completely shut down. Running only the left engine, the engine was accelerated up to full speed without experiencing engine stall. As will be seen later, this was not always the case, and even running a single engine, the engine sometime stalled, albeit at a speed of 80% and higher. However, at the time of the first test of a single engine it was viewed as proof that the engine stalls were not caused by the 'organ pipe' resonance or by a steady ingestion of exit hot gases. Therefore, the experimental effort was focused on double inlet instability, or more likely, on inlet flow distortions due to ground vortex ingestion, because engine stall problems had been reported in the past on aircraft using thrust reversing to assist braking (Ref. 5). It was decided to instrument the engine inlets with pressure modules for unsteady pressure measurements along the inlet duct walls to further investigate the problem.

2 Modules for unsteady pressure measurements

The NASA Glenn Research Center has multiyear experience with measurement of high frequency pressure oscillations in aircraft propulsion systems (Refs. 6, 7, and 8). In order to diagnose the reasons for engine stalls reliably, unsteady pressure oscillations inside the engine, in the inlets, and in front of the aircraft must be measured. However, in the case of the DP1 aircraft, no instrumentation was permitted inside the engines without revoking their flight worthiness. Therefore, only measurements inside the inlets, and in front of the aircraft were planned for. In the first phase of experiments the measurements were carried out in both engine inlets. Measurements of the flow field in front of the aircraft were planned for the second phase of experiments.

Miniature pressure transducers for measurements of high frequency pressure oscillations are very fine and fragile devices that must be treated very carefully to acquire reliable pressure data and secure longevity of these expensive instruments. In order to

achieve these goals, NASA engineers have adopted an approach of packaging miniature transducers into modules that allow easy installation, simple and reliable electric and pneumatic connections, quick removal for recalibration, and maximum transducer protection for mishandling and harsh environment.

The pressure modules, which were eventually installed in the inlets of aircraft DP-1C, were designed with the same philosophy as those developed for NASA testing. A drawing of the pressure module is shown in Fig. 2-1. The miniature pressure transducer (part 1 in Fig. 2-1) is mounted on a transducer bed (part 4) in such a way that the sensitive diaphragm of the transducer is about 1 mm away from the flow surface of the engine inlet. The transducer cover (part 5) protects the transducer against mishandling and supports electrical (part 6) as well as pneumatic (part 7) connectors. Fine electric wires and the back pressure tube of a miniature pressure transducer, both sensitive to possible damage, are attached to cover connectors and thus protected from the excessive loads often encountered with installations of bare transducers only. The electric wires and back pressure tube are not shown in Fig. 2-1. Components of a pressure module prior to assembly are shown in a photograph in Fig. 2-2, a pressure transducer mounted on the transducer bed is shown in Fig. 2-3, and finally a view of a partially assembled pressure module is in Fig. 2-4, where electric wires and connecting tubes to cover connectors are clearly visible.

After the assembly of the transducer module was completed, the cover side walls were closed with two lids. The metallic cover is also an excellent shield against electromagnetic interference. Two views of all pressure modules fabricated are in Figs. 2-5 and 2-6. Pressure modules were color coded and labeled for easy identification. All pressure transducers used had a range $\pm 35 \text{ kPa}$ ($\pm 5 \text{ psid}$). Modules labeled *WS1A, B, C* were furnished with Kulite transducers *XCS-190-5D*, modules *WS2A, B* were furnished with extended temperature range transducers Kulite *XTE-190-5D*. Finally module *WS3A1* was equipped with transducer *XCS-190-5D*; however the static tap had a larger diameter than the rest of the modules (1.5 mm versus 0.75 mm) in order to increase the frequency range of this module.

The pressure module also contains a conventional static tap the serves to verify the average pressure levels measured by the miniature pressure transducer. Transducer signals tend to drift sometimes, and therefore a ‘sanity’ check by the static pressure tap is highly recommended. Both pressure taps can be seen in Fig. 2-7 where a ‘flow’ face of a mounted pressure module is shown.

The pressure modules were mounted in the aircraft inlet on inserted base plates, as described in the following section. Overall dimensions of the transducer module assembly, including the base plate, are given in Fig. 2-1, indicating the space requirements needed for the installation of transducer modules.

3 Data acquisition setup and instrumentation layout

A schematic drawing of the entire data acquisition setup is shown in Fig. 3-1. The aircraft inlets were instrumented with six pressure modules (Pos. 1 in Fig. 3-1). The pressure transducers were powered and their signals were recorded by a National Instrument (NI) unit *PXI 1010* (Pos. 6). The connections were provided by four-wire shielded cables (Pos. 2). The pneumatic conventional taps were connected by tubing (Pos. 3) to individual Validyne *P855* pressure transducers (Pos.4). The low-frequency Validyne transducers were powered and their signals were recorded by the unit *PXI 1010* (Pos. 6) via shielded cables (Pos. 5). The data acquisition unit *PXI 1010* was controlled remotely by a NI unit *PXI 1000B* (Pos. 10), which was located in the Mobile Control Unit. The connection between both PXI units was provided via fiber optics cable (Pos. 7). Finally, both units were powered by an external generator (Pos. 9) supplying a voltage of 120 V via a grounded power cabled (Pos. 8).

Signals from rotational speed pickups *NI* (fan revolutions) for each engine were also acquired by the NI unit *PXI 1010*. Connections for these two signals are not shown in Fig. 3-1. All the signals acquired were recorded by the same unit, and therefore the signals have a common time datum base, and all the signals recorded are mutually synchronized.

A layout of the measurement ports made in both engine inlets is presented in Fig. 3-2; altogether 12 measurement ports were made. A table shown in Fig. 3-3 lists all the relevant dimensions. Pressure modules must be mounted flush with the flow surface to measure the wall static pressure correctly. Any protrusion or cavity at the module face, relative to the flow surface, will generate pressure fluctuations or at least noise levels that are not present in the undisturbed flow. The thickness of the DP-1 inlet cowling varies between 1.0 mm and 1.5 mm (40 and $60\text{ }\mu\text{inch}$). In addition to varying thickness, the cowling surface is curved. To assure that pressure modules are mounted correctly, it was decided to implant a metal base plate into the cowling, and to attach a pressure module to this base. The base plate is shown in Fig. 2-1 (part 3) and Fig. 3-4 (part 1). For a proper plate insertion, the edge of the central hole in the base plate was first aligned with the flow surface of the cowling, and then the plate was laminated to the cowling on the opposite surface of the cowling. By this method, all the base plates were correctly placed on the cowling even in locations where the curvature of the surface was quite high. A finished measurement port, ready for pressure module insertion, is shown in Fig. 3-5. Mounting of a pressure module in port *L030* is depicted in Fig. 3-6. Two pressure modules, mounted in ports *L030* and *L035*, with electrical and pneumatic connections in place are shown in Fig. 3-7. A view of a measurement port from inside an inlet duct with a pressure transducer inserted in the inlet wall was already shown in Fig. 2-7. Ports with base plates that were not used for a particular test run were closed with plugs flush with the inner wall of an inlet duct. An outside view of such plugs is shown in Fig. 3-8. A photograph of instrumented inlets prior mounting of the front cowling is in Fig. 3-9. Finally, Figs. 3-10 and 3-11 show the instrumented left and right inlets, respectively, with a front cowling mounted on the aircraft.

The main data acquisition unit *PXI-1010* was located on board the DP-1C aircraft. The photograph in Fig. 3-12 depicts the unit on the aircraft floor during shake down tests of communication with the main computer located in the Mobile Control Unit (MCU). For the actual testing, the unit was squeezed behind the pilot seat as seen in Fig. 3-13. An overall view of the entire test site is shown in Fig. 3-14; the MCU is on the left hand side of the photograph, the DP-1C aircraft in on the raised platform for the OGE testing. A view of the tested aircraft from the MCU cockpit is in Fig. 3-15. The controlling program for the instability tests was written in *LabVIEW 8.5*. An image of the main screen of the controlling program is captured in Fig. 3-16.

After unsteady pressure measurement tests were completed, the available ports were expected to be utilized for thermocouple probes to measure flow temperature distribution in the inlets in case that hot gas ingestion was encountered at high engine power settings. Unfortunately, these tests were not performed because of termination of the development program.

4 Overview of test conditions

The inlet instability tests were carried out for two basic ‘flight’ conditions: (1) out-of-the-ground effects (OGE) and (2) in-ground effects (IGE). The OGE tests were carried out on a raised platform with a deployed bare nose wheel (Fig. 4-1). The IGE tests were executed for three configurations: (1) a deployed bare nose wheel, (2) deployed faired nose wheel, and (3) removed nose wheel (simulating retracted nose undercarriage). The IGE test configurations are shown in Figs. 4-2 through 4-4.

A summary of selected test runs carried out during the inlet instability tests is presented in Figs. 4-5 through 4-8. The OGE tests carried out on the raised platform are presented in Fig. 4-5. As seen in this figure, the OGE tests were performed with both engines running simultaneously, as well as for a single engine, left or right, operating. The tests carried out on the ground (IGE) are presented in Fig. 4-6 for the deployed bare nose wheel, in Fig. 4-7 for the deployed faired nose wheel, and finally in Fig. 4-8 for the nose wheel removed.

No engine stalls were observed for the OGE conditions. For the IGE conditions, however, several engine stalls were recorded. There is no obvious pattern for engine stalls. From nine recorded engine stalls, seven stalls were experienced for the left engine and two stalls for the right engine. The engine stalls happened for engine speeds between 60% and 82%, with either both engines or a single engine running. Sometimes the engines ran at a higher speed than one for which they stalled in other runs. In one case, two stalls separated only by 300 ms occurred on the same engine. There was no detectable correlation of nose wheel configuration with engine stalling. The entire phenomenon of engine stalls appears to be somewhat random.

Several comments should be made about acquired and plotted parameters before analyzing the available data. The instantaneous engine speed was recorded by sampling

the frequency signal generated by the engine pick-up. The frequency of this signal is proportional to the engine speed, and its amplitude also varies somewhat with the engine speed. A conversion of digitized high frequency signal (6340 Hz for full engine speed) into engine speed required approximations that unfortunately added a certain jitter to the speed signal. The following two-step procedure was performed to minimize jitter in the engine speed signals. First, the entire speed signal record was subdivided into subintervals coincident with rotor revolution periods, and then average values for each rotor revolution were computed. Similar procedures were also applied to pressure signals in cases when it was desirable to improve plot readability by suppressing pressure fluctuations generated by passing fan blades.

5 Out-of-ground effect tests

Unsteady pressure measurements in the engine inlet ducts while the aircraft was placed on a raised platform served two purposes. First, the out-of-the-ground effect test runs were considered as shake-down tests for the entire data acquisition system and data reduction procedures. Secondly, the results acquired were used to establish a base line data set for the follow up IGE experiments.

There were no pop stalls recorded or observed for the out-of-the-ground effects while the both engines were operated up to 90% of the full speed. The unsteady pressure data, recorded at left engine inlet port *L030* were used to estimate the engine mass flow rate and inlet flow velocity as a function of engine speed. These estimates were based on a recorded ambient pressure, temperature, and humidity, and on a static pressure measured at a single port in the engine inlet. Consequently, the effects of possible non-uniform static pressure distribution around the inlet lip are not reflected in these estimated values. Measured engine mass flow rate and inlet flow velocity were corrected for the standard day conditions and are presented in Fig. 5-1. As seen in this figure the maximum corrected engine mass flow rate recorded was 46.3 kg/s for 90% of the engine speed, and the corresponding maximum inlet flow velocity was 198.2 m/s. The engine mass flow rate presented is in all likelihood slightly higher than the actual value, because no boundary layer effects, 'vena contracta', or possible flow separation around the inlet lip were considered here.

Unsteady pressure data from several test runs were subjected to a frequency analysis to investigate possible self induced flow oscillations in the engine inlet ducts. While performing the OGE tests, both engines were operated at several speeds that were kept constant during the data acquisition intervals. Frequency spectra of pressure fluctuations can easily be generated for constant test conditions. For a constant engine speed, a frequency line that is not associated with an engine order will be clearly detectable among shaft and blade passing harmonics. For the IGE tests, however, mostly transient data were recorded for variable engine speeds. The spectra for transient test runs do not show sharp frequency lines, the engine order harmonics are smeared over the range of speed variations, which masks all other frequency lines of interest. Therefore, only pressure spectra for the OGE test are presented here.

Unsteady pressure spectra for ports *L030* (inlet lip of the left engine) and *R050* (inlet lip of the right engine) are presented in plots in Fig. 5-2 and 5-3. These spectra were generated using data of test run *DI_02_19*. The upper plot in each figure is for the frequency range up to *12 kHz*, whereas the lower plot has a range to *4 kHz* only, which is just up to the first harmonic of the blade passing frequency for the given engine speed. The upper plots clearly show that the pressure oscillations at a frequency of the first and second harmonics of the fan blade passing frequency (BPF) propagate upstream through the entire inlet duct up to the lip. The right engine exhibits pressure oscillations that are a little more intense than those of the left engine. As seen in the lower plots, the harmonics of the rotor shaft frequency (RSF) are stronger for the right engine (Fig. 5-3), in particular the 3rd, 4th, 5th, 12th, 13th, and 16th harmonics. Of course the 17th RSF harmonic is also the 1st BPF harmonic. Asynchronous frequencies, that are not RSF or BPF harmonics, can be detected in pressure spectra of both engine inlets. These frequencies are labeled *A* for the left engine (Fig. 5-2), and *B* or *C* for the right engine (Fig. 5-3).

Spectra for three sensors located along the length of the left engine inlet duct (Ports *L030*, *L035*, and *L039*) are presented in Figs. 5-4 through 5-6. These spectra were generated for test run *DI_02_27*. On comparing the upper plots in these figures, it is obvious that the amplitude of the blade passing frequency (1st BPF) oscillations increases significantly closer to the engine fan face. The amplitude increases from *90 Pa* at the inlet lip (Port *L030*, Fig. 5-4) up to *420 Pa* just in front of the engine fan (Port *L039*, Fig. 5-6). Contrary to it, the RSF harmonics below the blade passing frequency, presented in lower plots, maintain more or less the same amplitudes. Amplitudes of asynchronous frequencies, labeled *D* and *E*, increase slightly closer to the engine fan. The origin of these asynchronous frequencies is not clear; their amplitudes are less than *10 Pa*. Flow or pressure disturbances of such small amplitude will not, for sure, instigate any engine instability, as is manifested by the smooth engine operation under the OGE conditions up to the full engine speed.

6 In-the-ground effect tests

As stated above, in-the-ground effect testing was carried out for three configuration of the aircraft nose undercarriage. These configurations were (1) deployed bare nose wheel, (2) deployed faired nose wheel, and (3) retracted (actually removed) nose wheel. Generally, no significant differences were found among these three configurations as far as engine stalls were concerned. All together, nine cases of engine stalls were recorded. Seven out of the nine recorded engine stalls occurred on the left engine, and only two stalls were recorded for the right engine. There was no case during this phase of testing, in which both engines stalled on the same test run.

6.1 Deployed bare nose wheel tests

In order to better understand the time sequence of pressure changes during an engine stall, test run *D1-04-18* will be explored in detail. The entire 20 s long run is depicted in Fig. 6-1. The plots show the history of speeds of both engines (the upper plot), the associated history of pressure changes recorded by four pressure transducers in the left inlet duct (the middle plot), and finally two pressure traces recorded in the right inlet duct. Locations of pressure transducer modules in both inlet ducts were presented in Fig. 3-2.

As seen in Fig. 6-1, both engines accelerated from about 60% to 70% speed, the left engine (red curve) being slightly faster. At about 72% speed, the left engine stalled (small dip in the red speed curve, arrow *A*), while the right engine was running smoothly. Approximately 1.5 seconds after the engine stall the pilot throttled back both engines (arrow *B*), and the engines decelerated to 25% speed. As seen in the middle plot, wall pressures in the left inlet duct were initially decreasing at the beginning of the record as the engine accelerated, and then a sudden pressure spike (arrow *C*) appeared indicating the engine stall. Wall pressure traces in the right inlet duct (the bottom plot) do not exhibit a pressure spike, which indicates no stalling of the right engine. After the engines were throttled down (arrows *D* and *E*), the wall pressures in both inlet ducts increased to nearly an ambient pressure level. Pressure levels measured close to the fan face (ports *L039* and *R099*) are slightly higher than pressure levels at the inlet lips (ports *L030* and *R050*) due to a mild diffusion of the inlet ducts.

To improve the time resolution and readability of the plots, the data are replotted for a smaller time interval centered about the pressure stall spike. First the time interval was reduced to 4 s, as shown in Fig. 6-2, and also the scale of fan revolutions was refined. A sudden drop in the speed of the left engine is now clearly visible (arrow *A*, red line). The fan velocity reaches its local minimum in about 0.2 s from the instant of the stall start, then the speed increases rapidly for about 0.3 s, and finally after additional 0.7 s the fan speed is back at its prestall level.

The time resolution was further increased to observe the changes in pressure signals. Figs. 6-3 and 6-4 depict time interval of 240 ms. The period of one engine revolution for the 70% speed is about 5.4 ms, which means that the plots depict an interval of 44 engine revolutions. Engine revolution averaging, as described above, is still suitable for engine speed graphs because of the relatively slow changes in the engine speed. However, in the case of pressure data such averaging may suppress important details in the fast changes of pressure fluctuations. Therefore, the pressure data in Fig. 6-3 is plotted as acquired. As seen in this figure, the pressure traces are very wide now, due to the fluctuations generated by fan blades. The width or ‘fuzziness’ of the traces is a measure of signal unsteadiness. For the left engine, the traces from all pressure transducers are of the same width. For the right engine, however, the situation is different. The signal measured in front of the fan (port *R099*) exhibits much higher unsteadiness than the one taken at the inlet lip (port *R050*). As stated earlier, the pressure transducer module plugged into port *R099* (*WS3A1*) was designed for a higher frequency

response than the rest of the modules, and thus it captures a wider spectrum of pressure fluctuations. To improve the graph readability, the pressure signals were filtered with a low pass filter with a cut-off frequency of 1000 Hz . A low pass filter removes high frequency fluctuations from a signal, but also introduces a certain small time delay. Because all the pressure data presented were filtered with the same cut-off filter, the time delay is identical for all the signals. Consequently, the mutual time relation among all pressure signals is not affected by filtering. Filtered data are presented in Fig. 6-4, where the individual pressure traces can be easily observed. There is no visible disturbance in pressure data of the left engine ahead of the engine stall (arrow *A*). There is an increased level of unsteadiness on the right engine pressure signals (arrow *B*), about 40 ms ahead of the left engine stall. It is not clear, however, if this had anything to do with the left engine stalling.

A sequence of pressure changes in the inlet duct can be detected in Fig. 6-5. The interval depicted in this plot is reduced to 60 ms . It is difficult to reconstruct the flow behavior based solely on the wall static pressure data (total pressure or velocity data would have been more definitive); nevertheless, the following scenario is most probable. Ahead of the pressure surge the pressure level in front of the fan is slightly higher than that at the inlet lip which indicates undisturbed flow through a mildly diffusing inlet duct (red line versus blue line). Once the engine stalls, a pressure burst (arrow *A*) propagates from the fan face (port *L039*, red line) through the inlet duct (port *L035*, green line) towards the inlet lip (ports *L030* and *L070*, dark and light blue lines). The pressure level in the entire duct increases significantly, and then for a short period the flow in the inlet duct stops (all pressures in the inlet duct are equal). While there is a little flow in the inlet duct, the pressure level in the entire duct is uniformly dropping (arrow *B*). After that, the pressure level at the fan face increases again (arrow *C*), whereas the pressures at the inlet lip and mid channel are more or less steady (disregarding small very low frequency oscillations), and close to the ambient pressure level (arrow *D*). Such a static pressure distribution may indicate reverse flow in the inlet duct, which lasts for about 30 ms (approximately 6 engine revolutions). Finally, the flow stops again (all pressures in the inlet duct are equal), and inflow in the fan starts again (arrow *E*) as the engine resumes normal operation.

The propagation speed of the pressure burst can be determined reliably by measuring the time interval for the pressure burst to travel from one measurement port to another. As indicated in Fig. 6-6, the pressure burst for a pressure level of $\pi_x = 1.05$ spreads from port *L039* to port *L035* in 0.947 ms , and it takes an additional 1.073 ms for the burst to reach port *L030*. The average propagation velocity of the pressure burst is 289.2 m/s (948.8 fps). This is a propagation velocity relative to the inlet surface, not relative to the incoming flow; of course, a pressure disturbance propagates in air with the speed of sound, which in the case of test *DI_04_18* was about 349 m/s , based on the measured total (ambient) temperature of 303 K . The measured speed of the pressure burst relative to the inlet walls was 289 m/s , which implies that the air inlet velocity could not be higher than 60 m/s . In the case of the OGE operation (Fig. 5.1) the inlet flow velocity was about 135 m/s at the relative engine speed of 72%. Obviously, the pop stall occurrence must decrease the inlet flow velocity significantly.

Variations of the inlet flow velocity for the pop stall occurrence were calculated using a wall pressure signal detected at port *L030*, and the measured ambient (total) conditions. A procedure similar to that used to determine the engine mass flow rate for the OGE tests (Fig. 5.1) was employed again, this time however for the unsteady static pressure input. Results of these calculations are presented in Fig. 6-7. As seen here, the inlet flow velocity, and consequently also the engine mass flow rate, drops to zero or even to very low negative values, for a short period of about *5 ms*, just after the pressure burst reaches the inlet duct lip. During *2 ms* of this rapid inlet velocity deceleration from about *130 m/s* to zero was an instant when the inlet velocity passed the level of *60 m/s*, which most likely was the instant for which the burst propagation velocity of *289 m/s* was determined. Results presented in Fig. 6.7 correlate very well with the description of inlet flow behavior, which was based on pressure changes depicted in Fig. 6-6, and was described above.

Values of the mass flow rate and inlet velocity during the instant of the pop stall back flow appear to be extremely high; however, it all happens in a very short time interval. The design pressure ratio of the PWC 535A engine is about *1.84*, thus there is a sufficient pressure buildup behind the fan rotor to drive the flow back once the fan is stalled. Also, the back flow through the inlet duct lasts for only about *5 ms*, and during that period the accumulated air mass pushed back through the inlet is less than *0.15 kg*.

Finally, the shortest segment of data (*6 ms*) presented in Fig 6-6 is shown once again in Fig. 6-8; however, this time unfiltered data are shown. As seen in this figure, in particular in the data for the right engine, the data acquisition setup has a sufficiently high sampling frequency to distinguish blade potential flow fluctuations ahead of the engine fan. As marked in this figure, effects of all *17* blades are clearly captured during one fan revolution. It is worthwhile to note that the fan blade potential flow fluctuations can be detected as far as at the inlet lip (port *R050*).

6.2 Deployed faired nose wheel tests

Two out of the nine recorded engine stalls occurred on the right engine. One of these stalls, which occurred for the configuration with the faired nose wheel, is depicted in Figs. 6-9 and 6-10. Basically, there is no visible difference in the right engine response to an inlet disturbance compared to the left engine response. Engine stall was manifested by a rapid drop in the engine revolution level (arrow *A* in Fig. 6-9), followed by a recovery to normal operation conditions. As in all previous cases this recovery was interrupted by throttling the engines. The right engine stall is replotted on a finer time scale in Fig. 6-10. The pressure trace recorded at the inlet port close to the fan face (port *R099*) exhibits higher instabilities than was the case for a similar port on the left inlet (port *L039*). The reason for it is the wider frequency range of the *WS3A1* pressure module as discussed earlier.

6.3 Retracted nose wheel tests

An extremely interesting data set was recorded for the configuration with the nose wheel retracted (record *DI-03-18*). During this test run, two pop stalls were recorded as presented in Fig. 6-11 (arrows *A* and *B*). The left engine stalled twice in a row, with only *256 ms* separating the stalls, as depicted in Fig. 6-12. The stall pressure bursts are labeled *Stall A* and *Stall B* for later identification. Surprisingly, *Stall B* occurred during the recovery phase of *Stall A* at visibly lower engine speed than the one at the *Stall A* instant. This may indicate that engine stalls are not set off by continuous or a long time scale event, but by some sudden intermittent disturbance in the inlet flow. If, for example, the engine stall is set off by a ground vortex intrusion in the inlet, then in this case the pressure burst and outflow from the inlet generated by *Stall A* did not blow the ground vortex away from the inlet, but the vortex returned back in the inlet, set the *Stall B*, and then finally was blown away by the burst generated by *Stall B*. It appears that after *Stall B*, the engine was recovering to normal operation, but was terminated by throttling both engines (arrow *C* in Fig. 6-11).

7 Summary of in-the-ground effect tests

In-the-ground effect test runs for all three nose wheel configurations for which engine stalls were recorded are summarized in Figs. 7-1 and 7-2 for the left engine and for the right engine, respectively. Segments of data *60 ms* long were chosen for this comparison. The charts in these figures are arranged in an increasing order of the stall engine speed, regardless of nose wheel configuration. The nose wheel configuration is marked in each chart. Also, the test run labels are given in each chart which allows a quick cross reference to the summary of test runs presented in Figs 4-6 through 4-8. Viewing the charts in Figs 7-1 and 7-2 clearly indicates that the nose wheel configuration has little or no effect on the engine stall response and its effect on the inlet flowfield fluctuations. The character of the inlet flowfield is basically the same for all the data sets presented, except that the intensity of the pressure fluctuations increases with increasing engine speed at which the stall occurred. As seen in the lowest two charts in Fig. 7-1 (left engine running alone and stalling at *80%* speed and higher), the intense pressure fluctuations detected in front of the fan face (port *L039*, red line) spread upstream even beyond the mid point of the inlet duct (port *L035*, green line). A rough estimate of the period of these fluctuations and its ratio to the engine revolution period indicates that these fluctuations are probably generated by a rotating stall cell on the fan rotor. For example, for the left engine at *82.7%* speed (*DI-03-42*), the ratio of periods is *45%*, and for the right engine at *67.8%* speed (*DI-04-07*), the ratio is *28%*. These values are within a commonly accepted range of rotating stall cell speed to engine shaft speed ratio of *25%* to *60%*.

An important fact to be noticed in these figures is that there is no detected instability in the inlet duct wall static pressures prior to the arrival of pressure bursts caused by to engine stalls. It is true that only *10 ms* of data (about two engine revolutions) are shown ahead of the burst, but no static pressure instability was observed

even for several seconds of data ahead of the stall (e.g. Figs. 6-8 and 6-10). It appears that the inlet disturbance which leads to engine stalls is not manifested by changes in the wall static pressure distribution of the inlet flow. Also, it should be mentioned that stalls of both engines at the same time were never recorded.

The facts stated above indicate that engine stalls are probably evoked by a sudden ingestion of a vortex generated between the two streams moving in opposite directions: outbound hot gas stream from the main nozzle close to the ground and inbound inlet flow above. At a certain velocity ratio of these two streams, which is a function of engine speed, the vortex reaches an intensity level at which the left or the right end of the vortex attaches to a firm surface (either ground or the surface of the aircraft) and the other end is swallowed by one of the aircraft inlets. Once the vortex enters the inlet duct a puff of hot air can be sucked through the vortex core into the engine. Because the vortex core size is significantly smaller than the inlet diameter, wall static pressures on the inlet inner walls are not or only very little affected by the vortex presence. Once the engine stalls, the outflow from the inlet pushes the vortex away and the engine resumes normal operation. Because the engines were always throttled down after the pilot heard the pop noise, it is difficult to predict what would happen next. Of course this is just a hypothesis based on circumstantial evidence. Extensive smoke flow visualization ahead of the aircraft inlets, accompanied by velocity and unsteady total pressure measurements in the inlets are needed to provide a full explanation of the causes for engine stalls, and suggest corrective measures to ensure flawless operation of the engines at full power while the aircraft is in close proximity to the ground.

References

1. DuPont, A.A. and Reuss, R.P.: "Testing an Inlet for a Twin Engine VTOL Aircraft," Paper ISABE 2003-1112, Sep. 2003.
2. Bell Aircraft Corporation: "X-14 Research Airplane Summary Report," Report no. 68-989-004, Sep. 1958.
3. Saripalli, K.R., Flood, J.D., and Moss, G.M.: "Inlet Hot Gas Ingestion (HGI) and Its Control in V/STOL Aircraft," AIAA Paper 975517, 1997.
4. DuPont, A.A.: "Tethered Hover of DP-1C Test Aircraft," Final report, ONR Contract no. N00014-07-C-0385, Dec. 2007.
5. Motycka, D.L.: "Ground Vortex – Limit to Engine/Reverse Operation," Transaction of the ASME, Journal of Engineering for Power, pp. 258-264, Apr. 1976.
6. Lepicovsky, J. et al: "Methodology of Blade Unsteady Pressure Measurement in the NASA Transonic Flutter Cascade," NASA/TM—2002-211894, Oct. 2002.
7. Lepicovsky, J. and Braunscheidel, E.P.: "Measurement of Flow Pattern Within a Rotating Stall Cell in an Axial Compressor," NASA/TM—2006-214270, Jun. 2006.
8. Lepicovsky, J.: "Unsteady Velocity Measurements in the NASA Research Low Speed Axial Compressor", NASA/CR—2007-214815, May 2007.



Fig. 1-1 DP-1C aircraft on an elevated platform for OGE testing.



Fig. 1-2 Inlet fence to prevent hot gas ingestion.

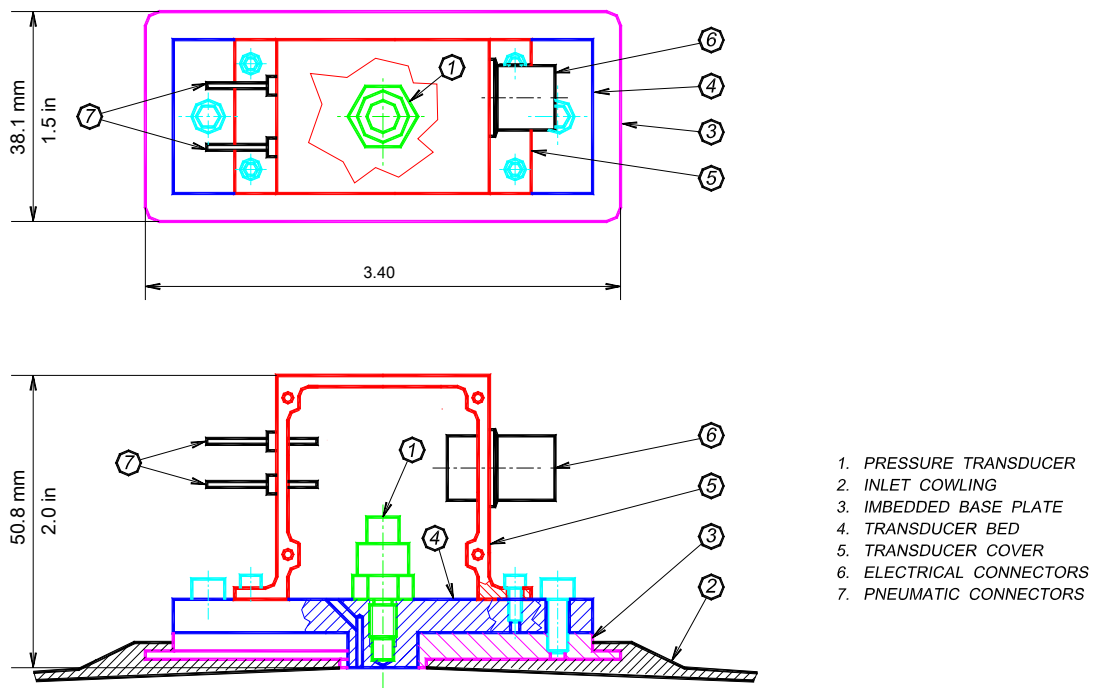


Fig. 2-1 Transducer module assembly for DP-1C tests.

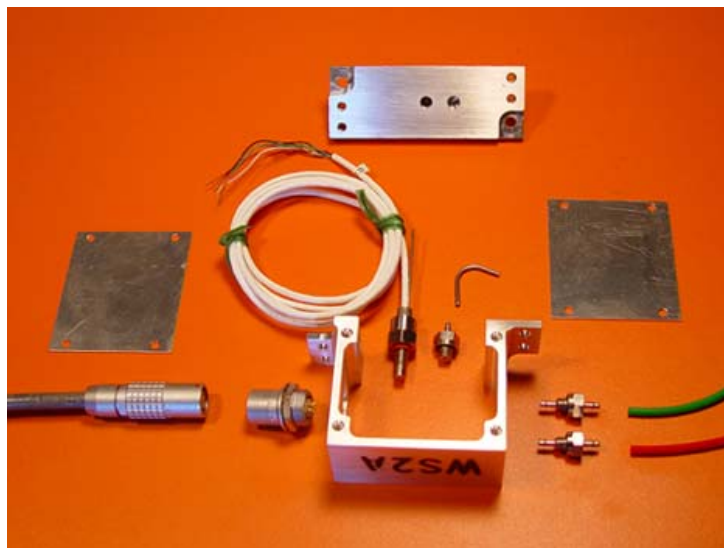


Fig. 2-2 Components of the transducer module.

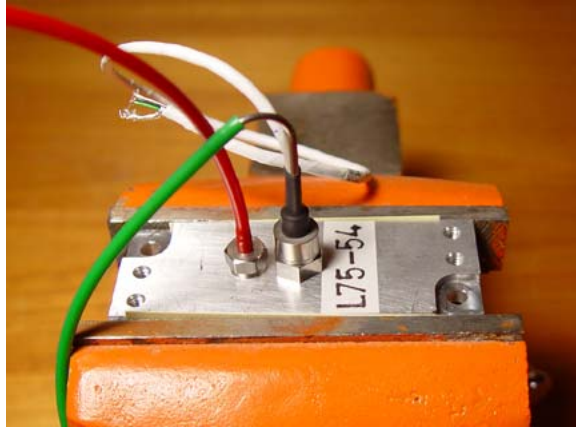


Fig. 2-3 Wall pressure module under construction.

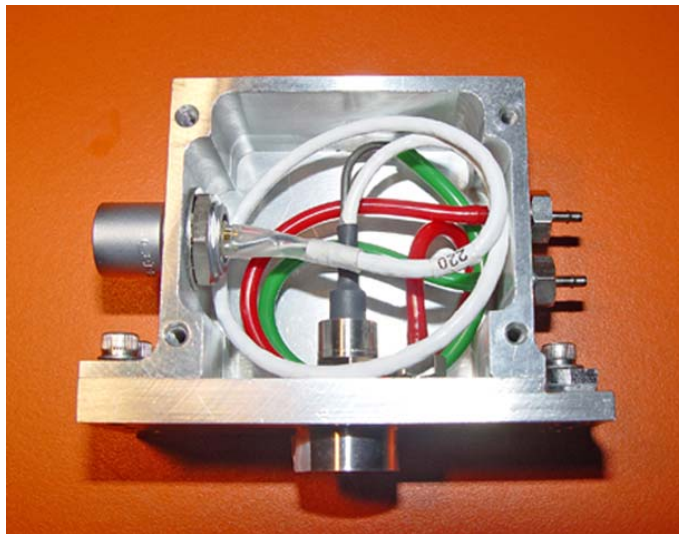


Fig. 2-4 Partially assembled wall pressure module.

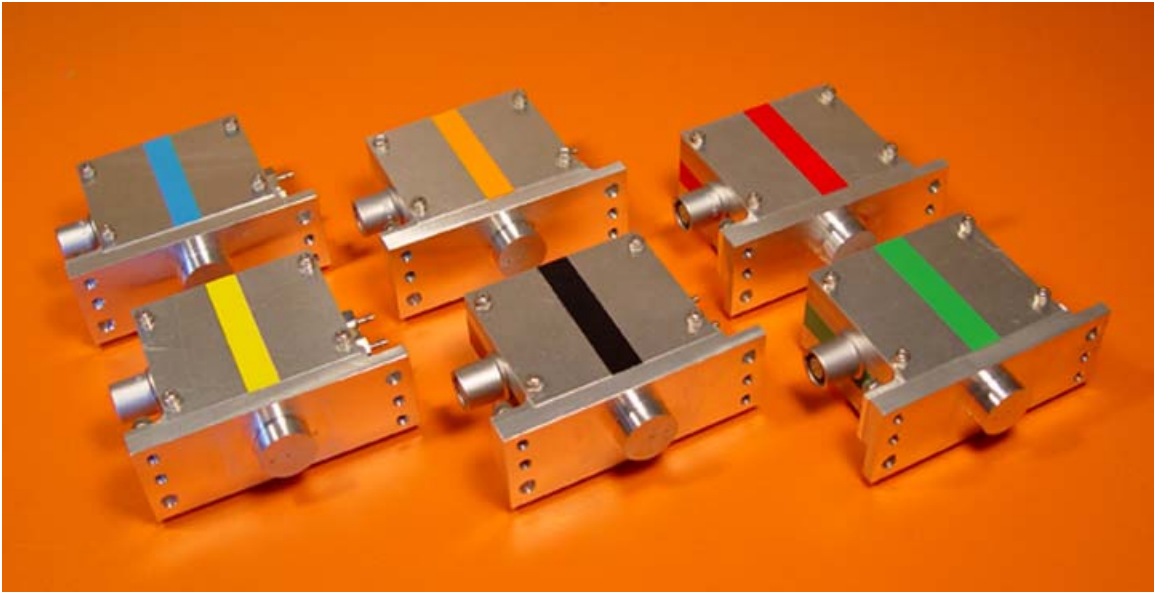


Fig. 2-5 Assembled wall pressure modules (side view).



Fig. 2-6 Assembled wall pressure modules (view from 'pneumatic end').

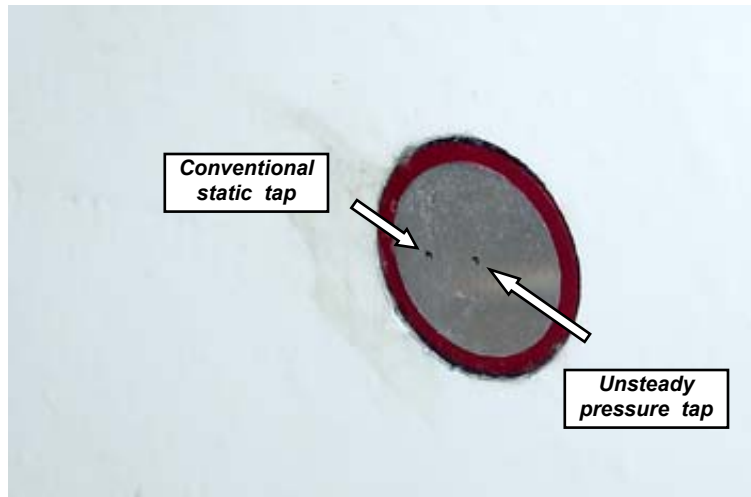


Fig. 2-7 Pressure module mounted in an inlet wall (view from inlet).

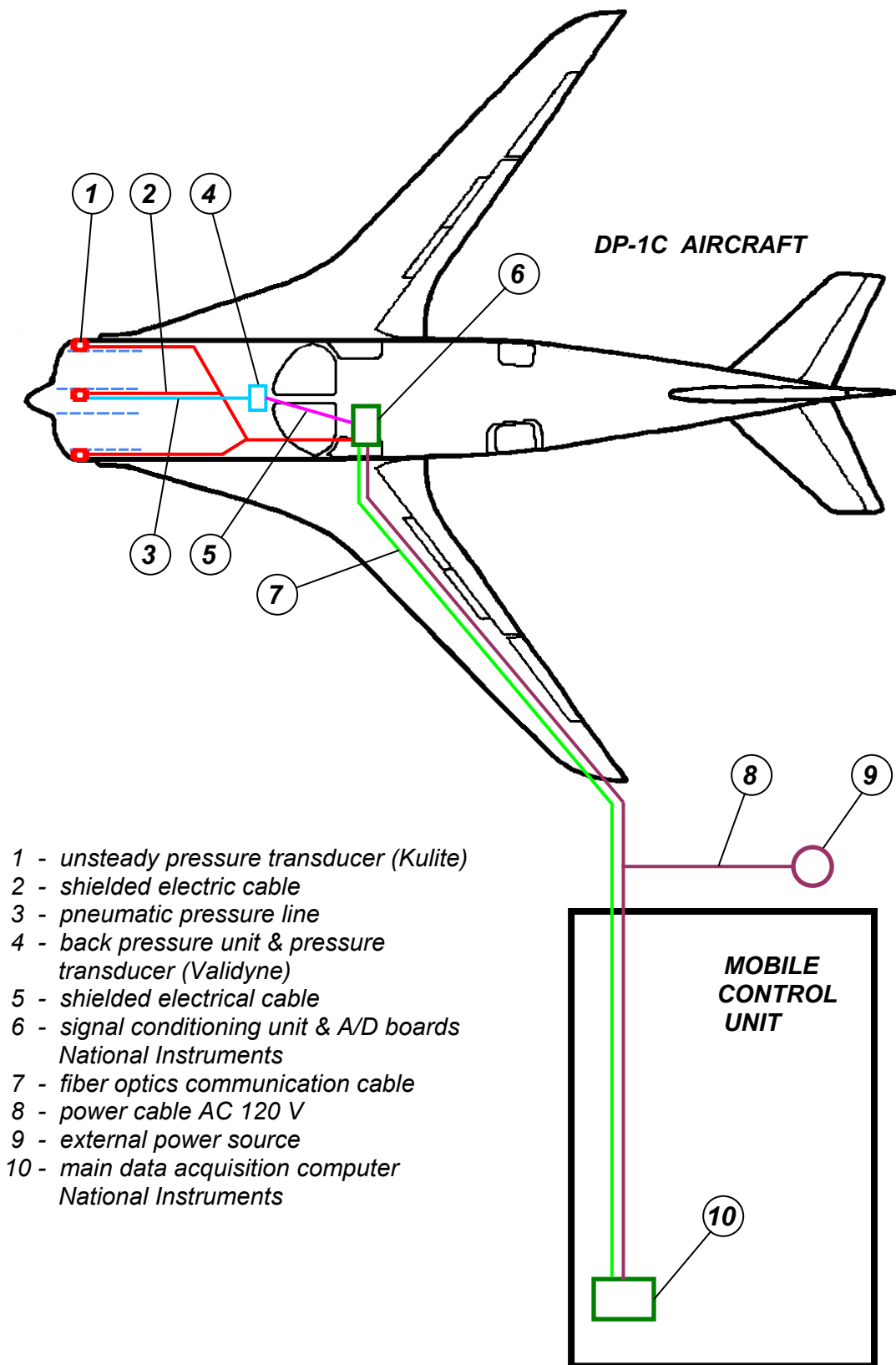


Fig. 3-1 Basic instrumentation layout for DP-1C inlet instability tests.

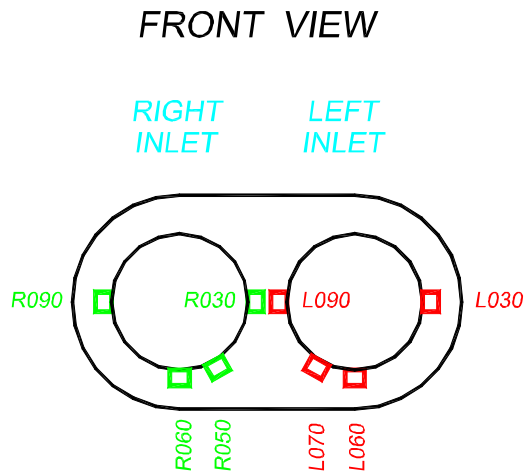
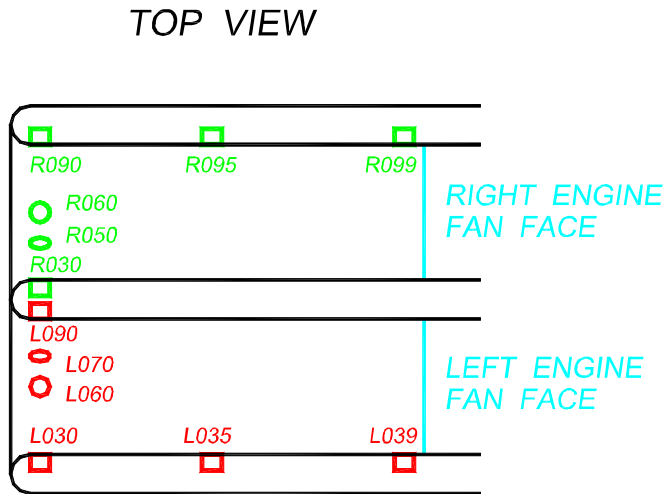


Fig. 3-2 Layout of measurement ports in DP-1C inlets.

LEFT ENGINE

PORT	L090	L070	L060	L030	L035	L039
x (mm)	678	654	652	654	421	121
x (in)	26.69	25.75	25.69	25.75	16.56	4.75
alfa (dg)	255	210	168	80	83	83
alfa (hr)	8:30	7:00	5:35	2:40	2:45	2:45

RIGHT ENGINE

PORT	R090	R060	R050	R030	R095	R099
x (mm)	705	667	673	715	416	127
x (in)	27.75	26.25	26.50	28.13	16.38	5.00
alfa (dg)	270	188	150	75	270	275
alfa (hr)	9:00	6:15	5:00	2:30	9:00	9:10

x = DISTANCE FROM THE FAN FRONT FACE
 alfa = CLOCKWISE ANGLE

DIAMETER OF FAN FRON FACE 580 mm (22.85 in)
 INLET DIAMETER AT PORT L030 540 mm (21.26 in)

Fig. 3-3 Coordinates of access ports.

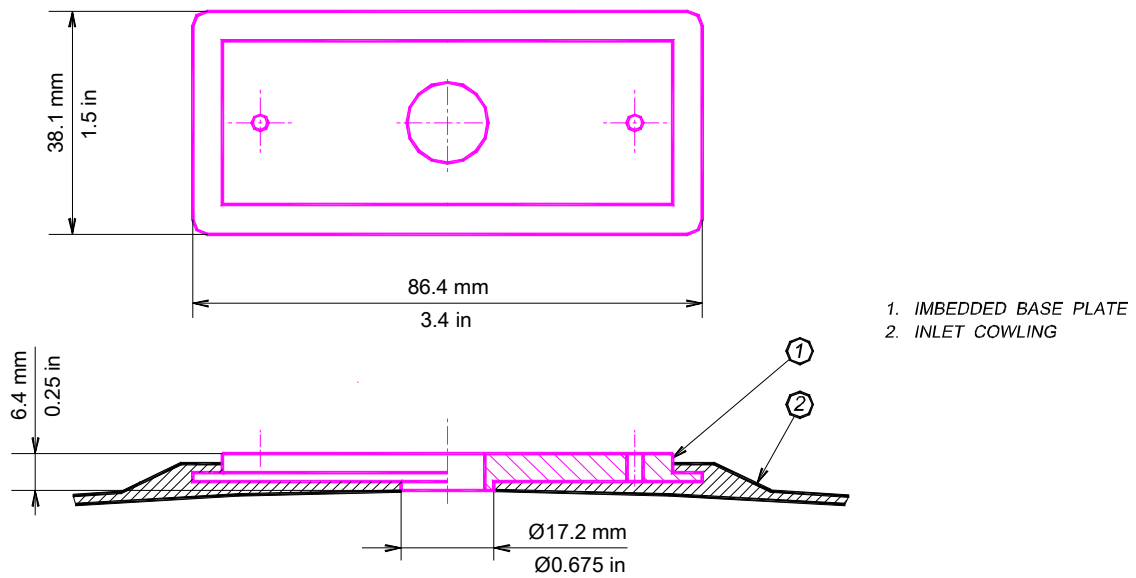


Fig. 3-4 Base plate laminated to inlet cowling.



Fig. 3-5 Access port in the left inlet wall (view from inside of inlet duct).



Fig. 3-6 Mounting of pressure module on the outer side of an inlet wall.



Fig. 3-7 Pressure modules plugged into ports L030 and L035.



Fig. 3-8 Unused access ports closed with wall plugs.



Fig. 3-9 View of instrumented inlets with front cowling removed.



Fig. 3-10 Fully instrumented left engine inlet.



Fig. 3-11 Fully instrumented right engine inlet.



Fig. 3-12 Data acquisition unit *PXI-1010* on board during shake down tests.



Fig. 3-13 Unit *PXI-1010* at its final location behind the pilot seat.



Fig. 3-14 Overall view of the test site with the mobile control unit on the left.



Fig. 3-15 View of the tested aircraft from the cockpit of the mobile control unit.

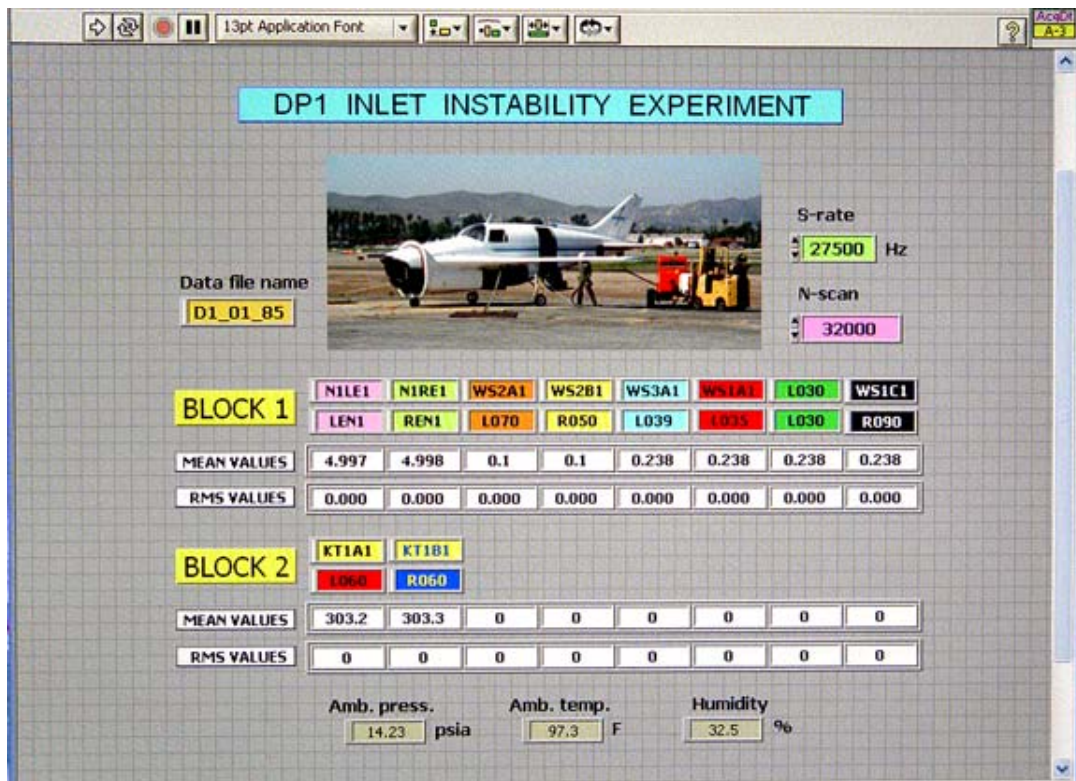


Fig. 3-16 Captured screen of the controlling *LabVIEW* program.



Fig. 4-1 Configuration with deployed bare nose wheel for out-of-the-ground effect tests.

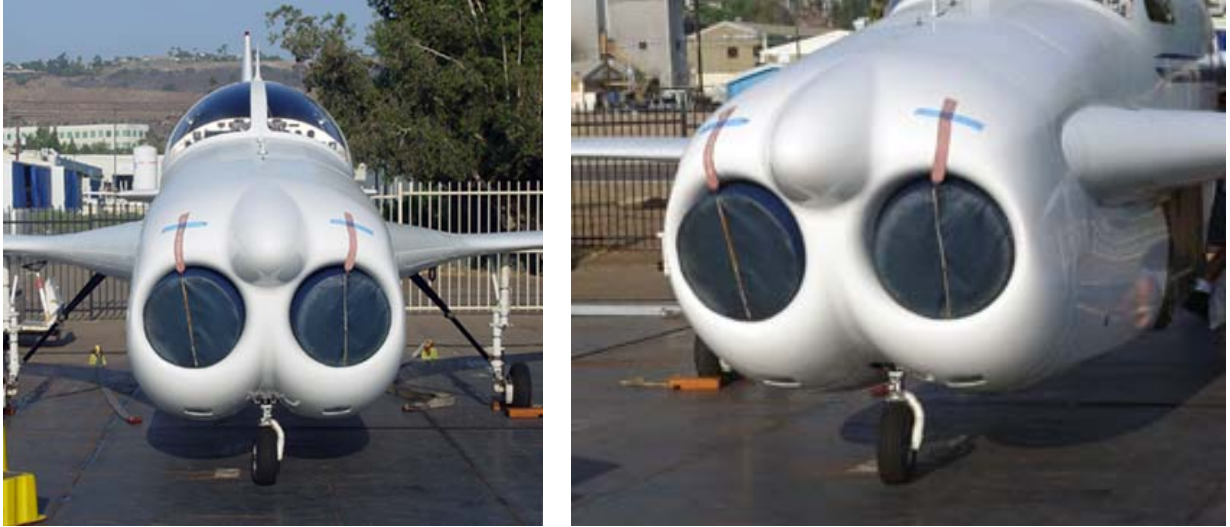


Fig. 4-2 Configuration with deployed bare nose wheel for in ground effect tests.



Fig. 4-3 Configuration with deployed faired nose wheel for in ground effect tests.



Fig. 4-4 Configuration with removed nose wheel for in ground effect tests.

BARE NOSE WHEEL

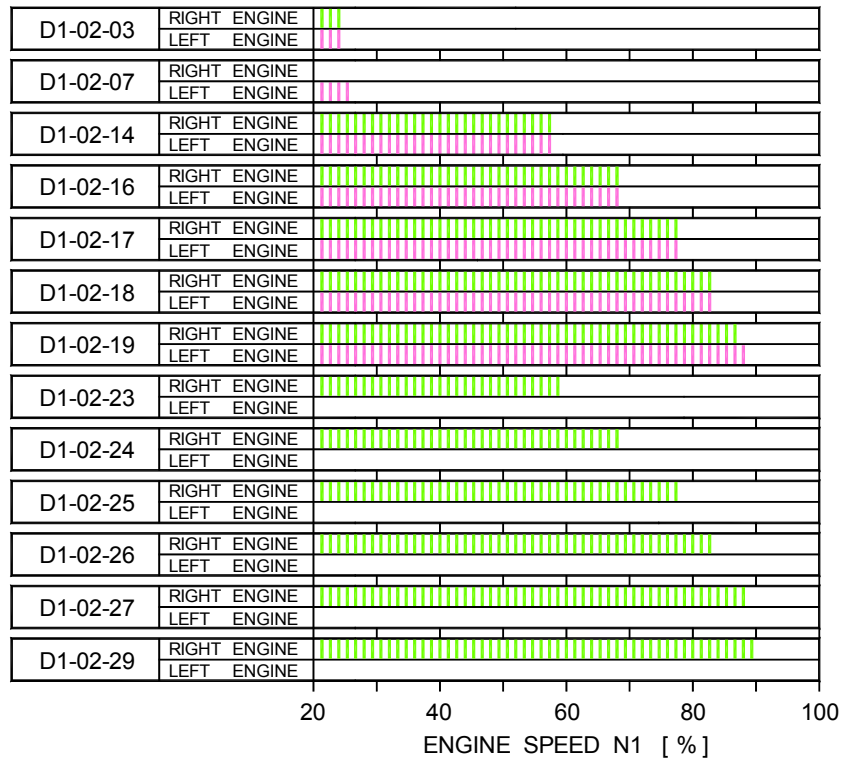


Fig. 4-5 Out-of-the-ground effects -- selected test conditions for deployed bare nose wheel.

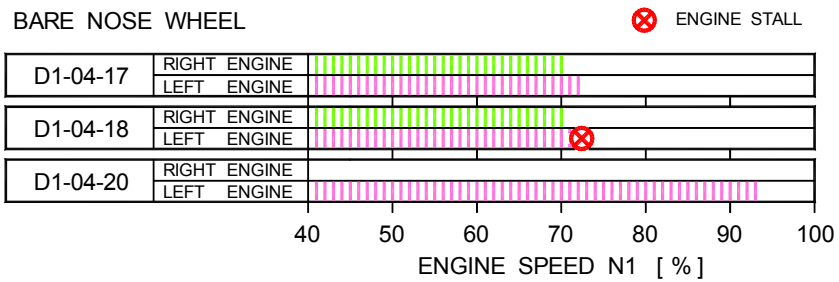


Fig. 4-6 In-ground effects -- selected test conditions for deployed bare nose wheel.

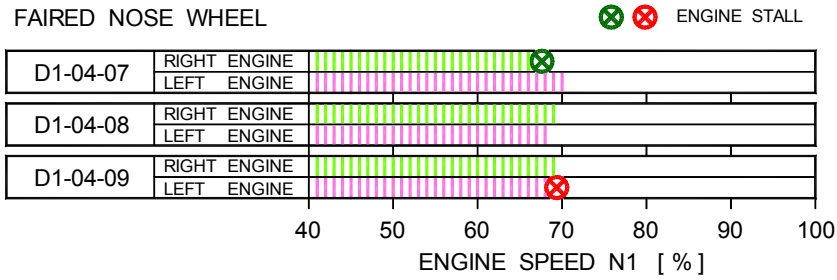


Fig. 4-7 In-ground effects -- selected test conditions for deployed faired nose wheel.

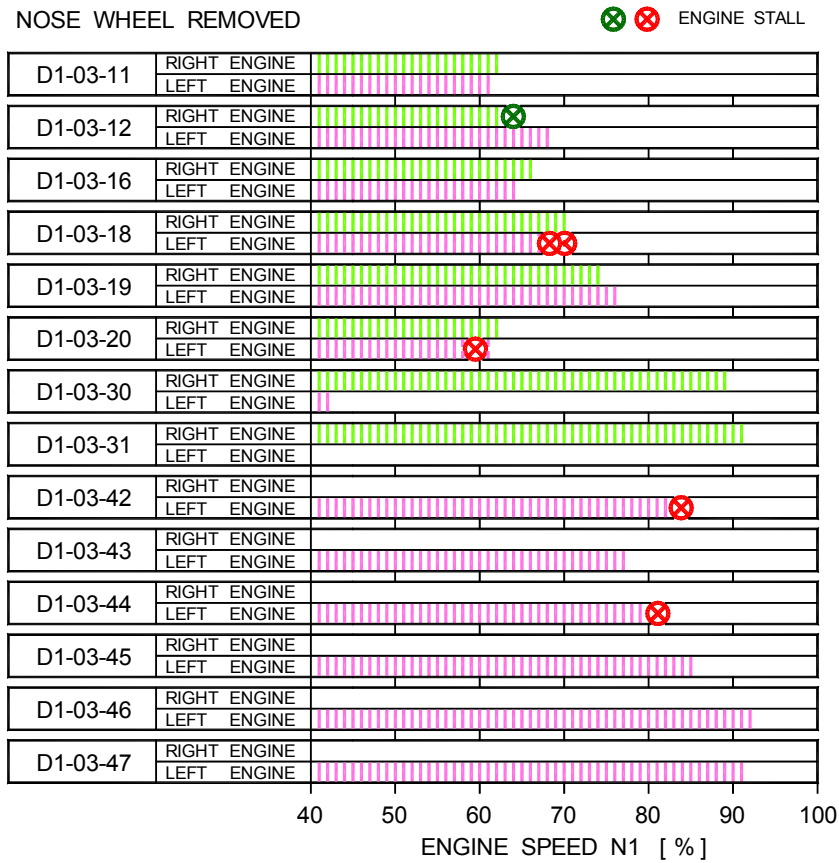


Fig. 4-8 In-ground effects -- selected test conditions for nose wheel removed (retracted).

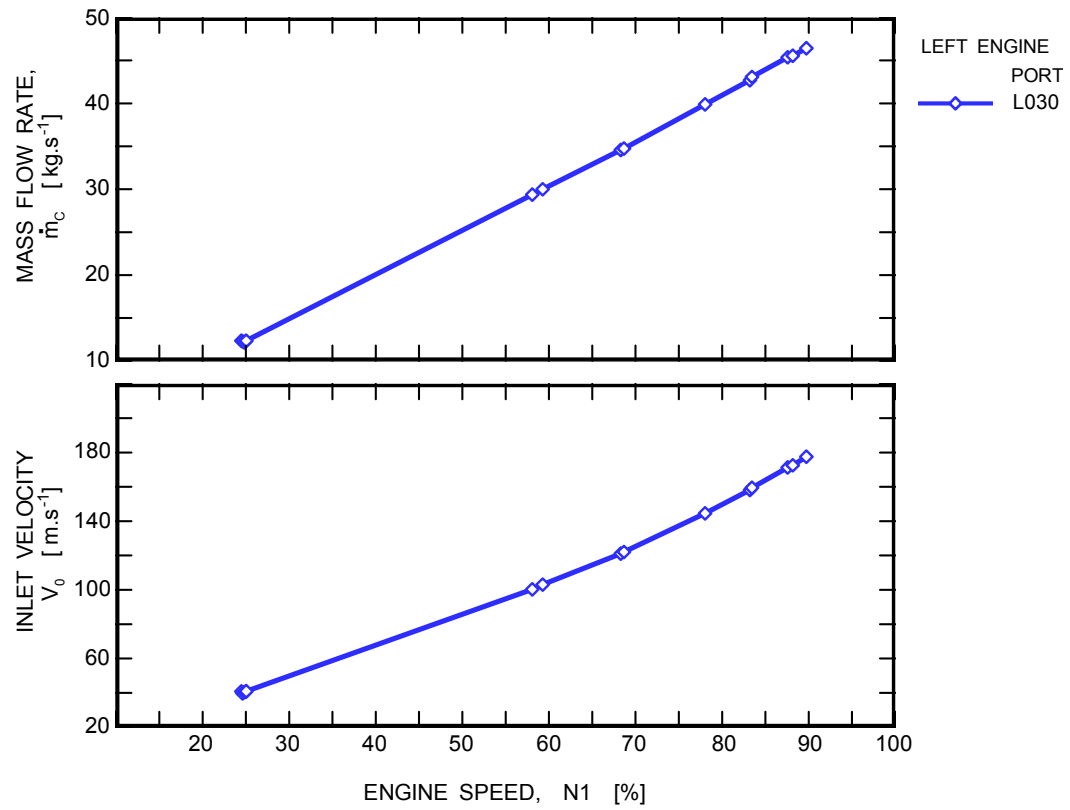


Fig. 5-1 Engine mass flow rate and inlet flow velocity as functions of engine speed.

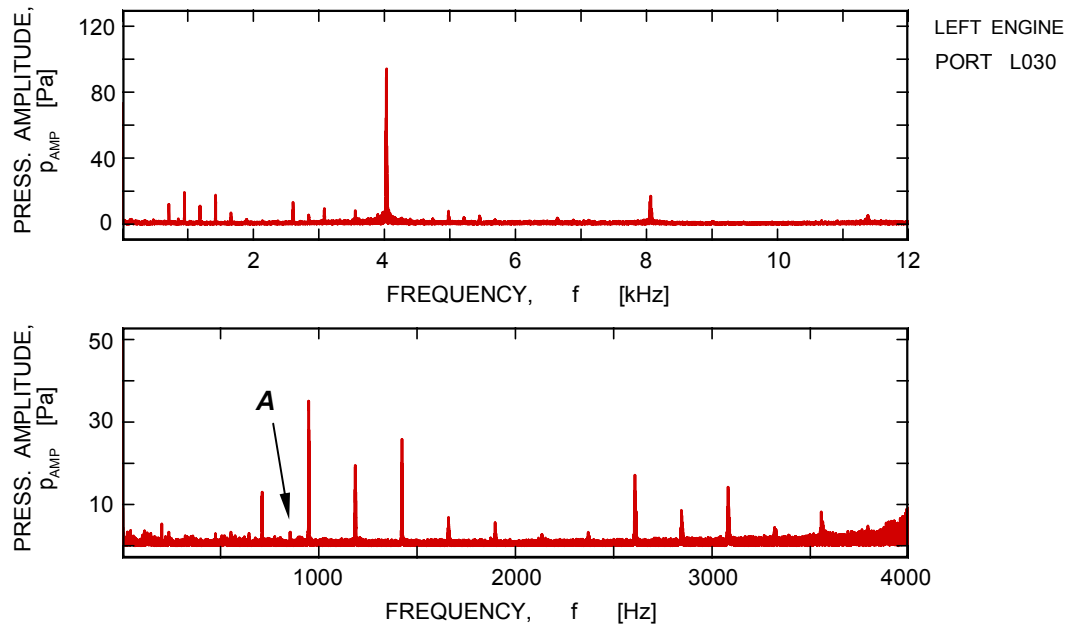


Fig. 5-2 Frequency spectra of pressure fluctuations taken at port *L030* for left engine speed *NI* of 87.5 % (test run *D1_02_19*).

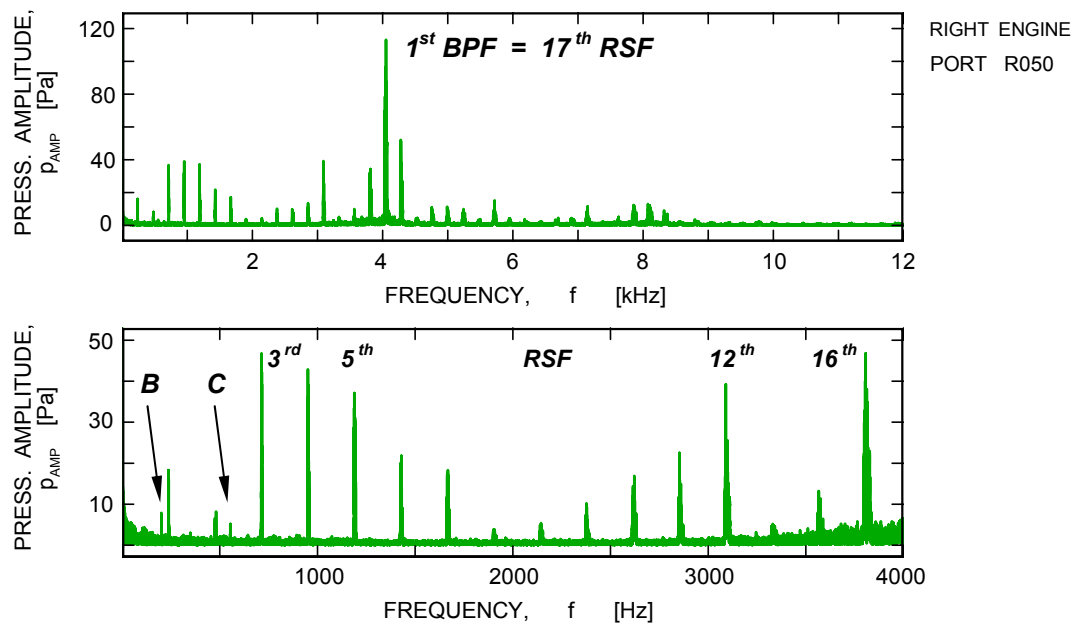


Fig. 5-3 Frequency spectra of pressure fluctuations taken at port *R050* for right engine speed *NI* of 87.9 % (test run *D1_02_19*).

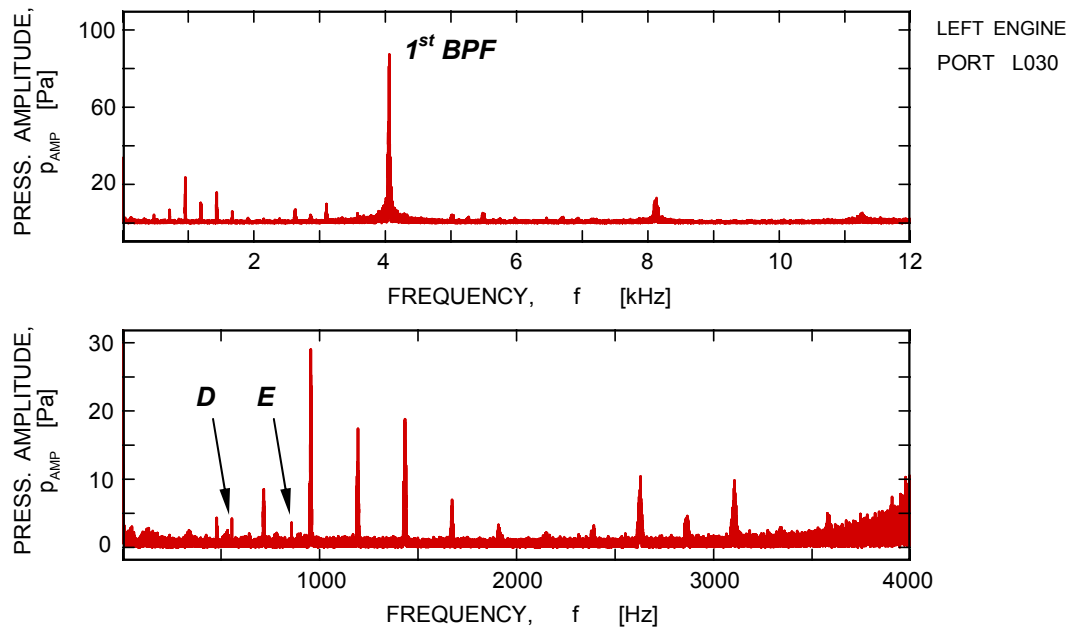


Fig. 5-4 Frequency spectra of pressure fluctuations taken at port *L030* for left engine speed *NI* of 88.2 % (test run *D1_02_27*).

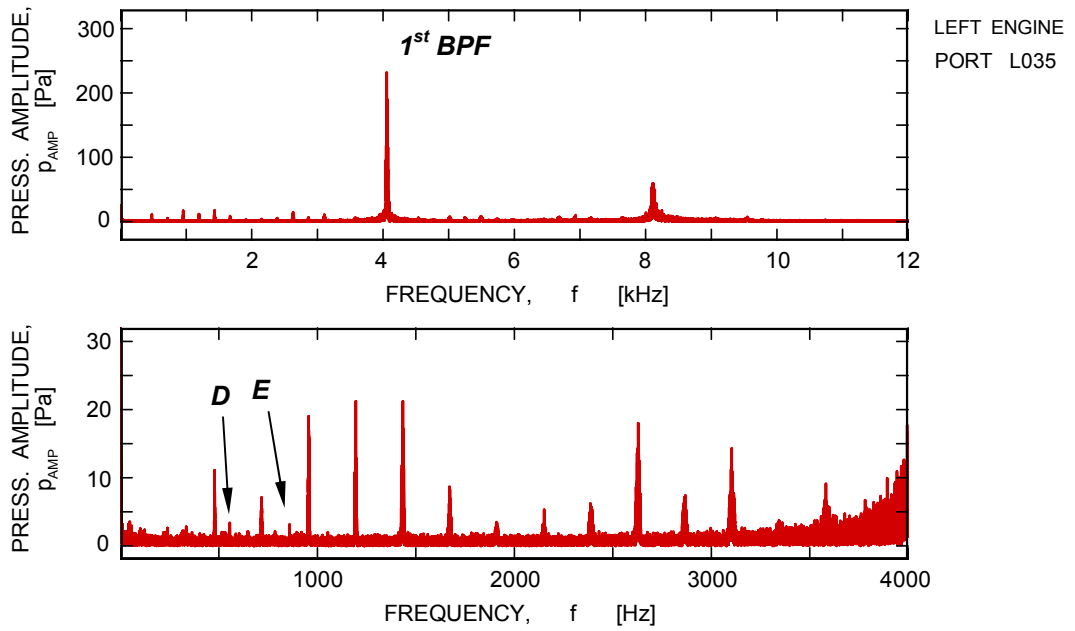


Fig. 5-5 Frequency spectra of pressure fluctuations taken at port *L035* for left engine speed *NI* of 88.2 % (test run *D1_02_27*).

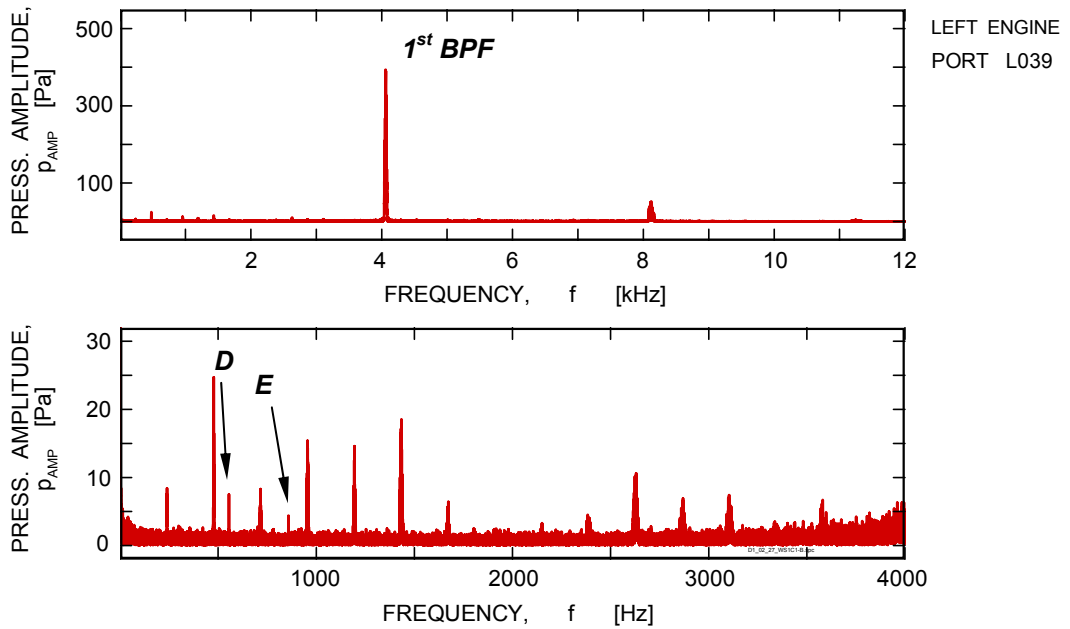


Fig. 5-6 Frequency spectra of pressure fluctuations taken at port *L039* for left engine speed *NI* of 88.2 % (test run *D1_02_27*).

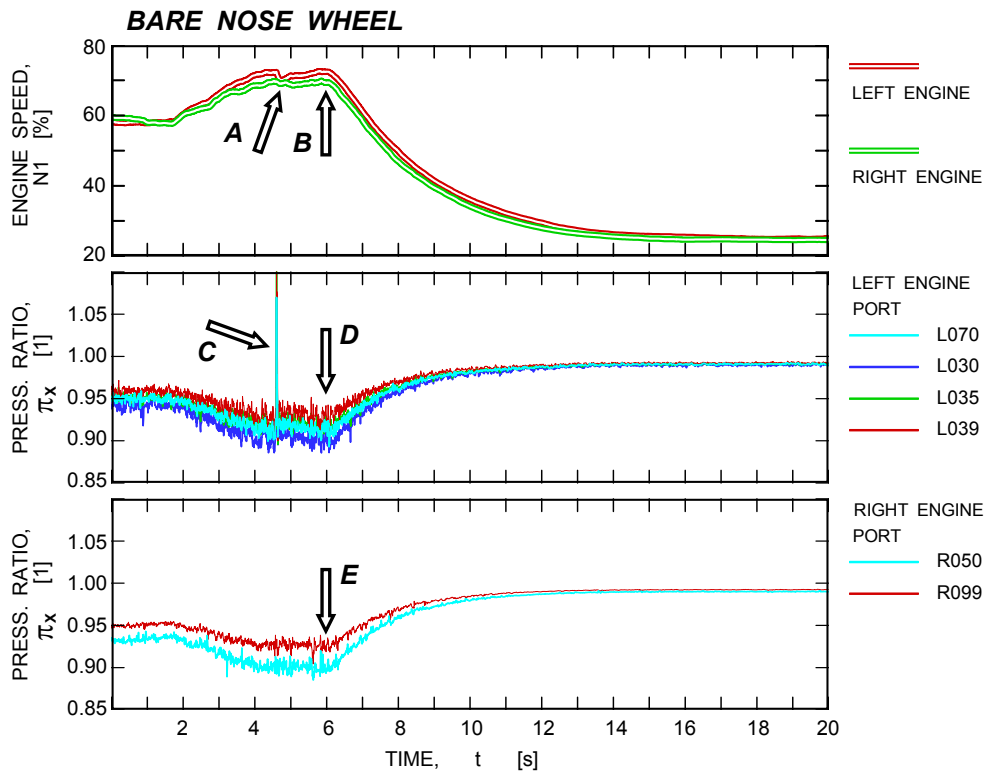


Fig. 6-1 Engine stall test D1-04-18; entire recorded segment of 20 s.

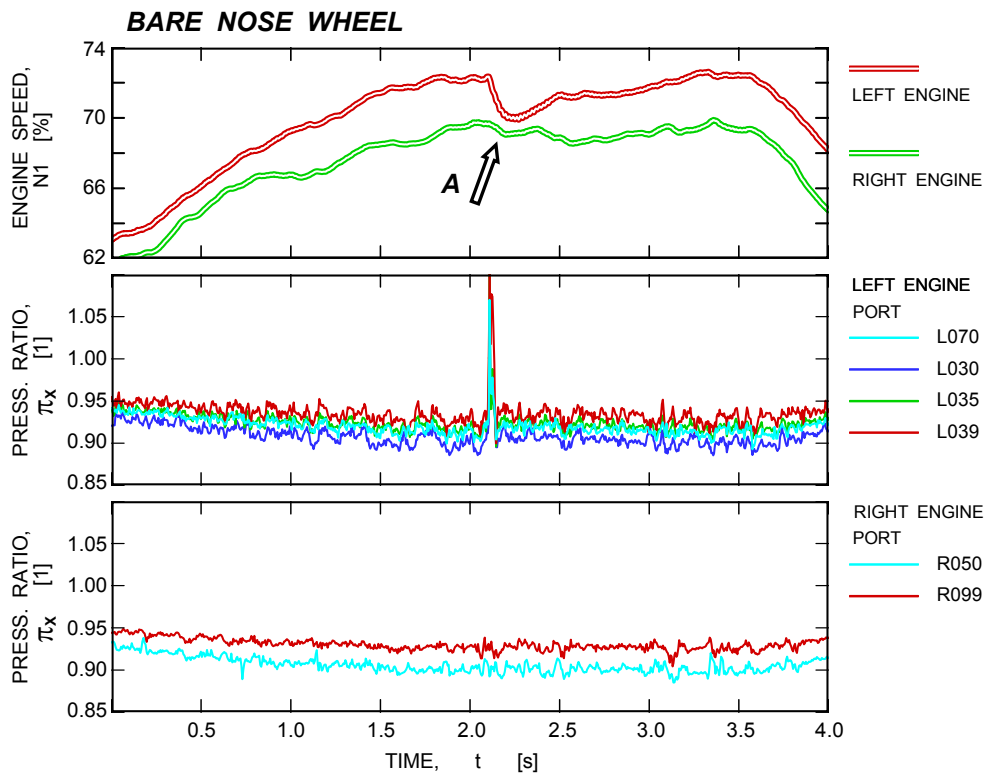


Fig. 6-2 Engine stall test D1-04-18; plotted time interval of 4 s.

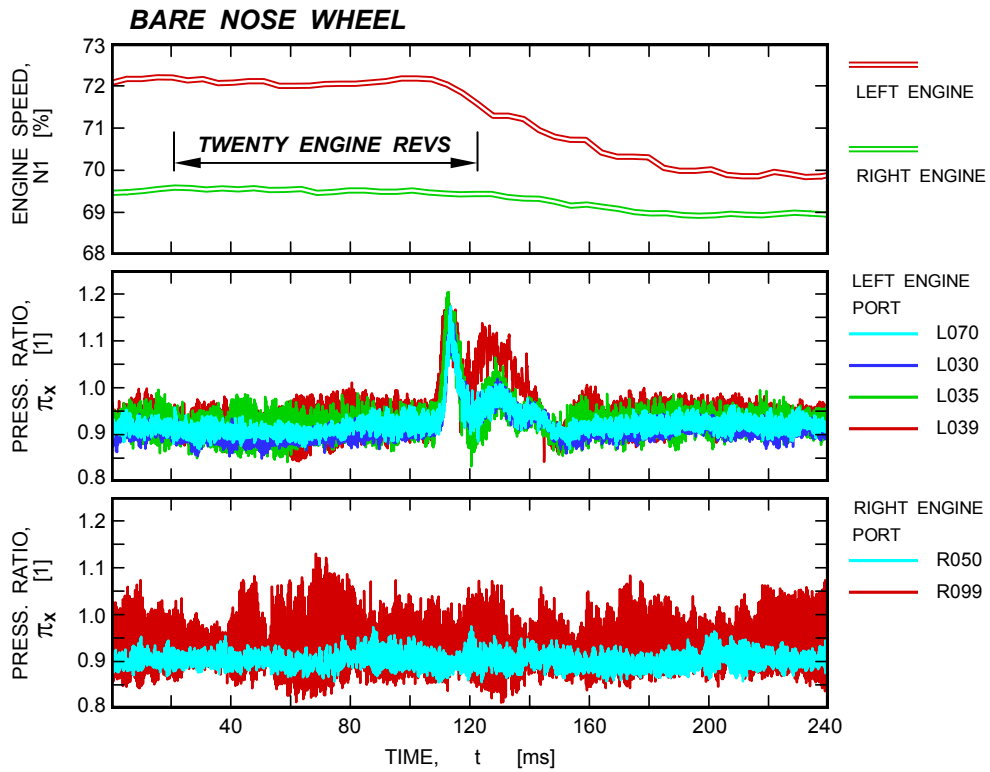


Fig. 6-3 Engine stall test *D1-04-18*; plotted time interval of 240 ms; unfiltered pressure data.

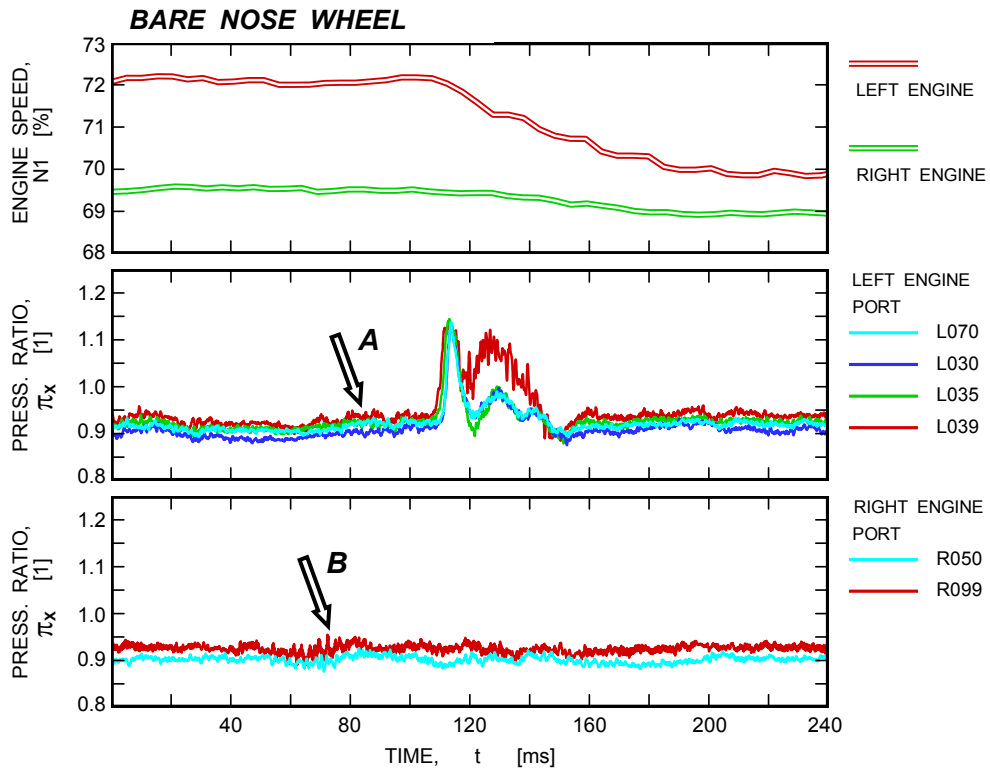


Fig. 6-4 Engine stall test *D1-04-18*; plotted time interval of 240 ms; filtered pressure data $f_{LP} = 1000$ Hz.

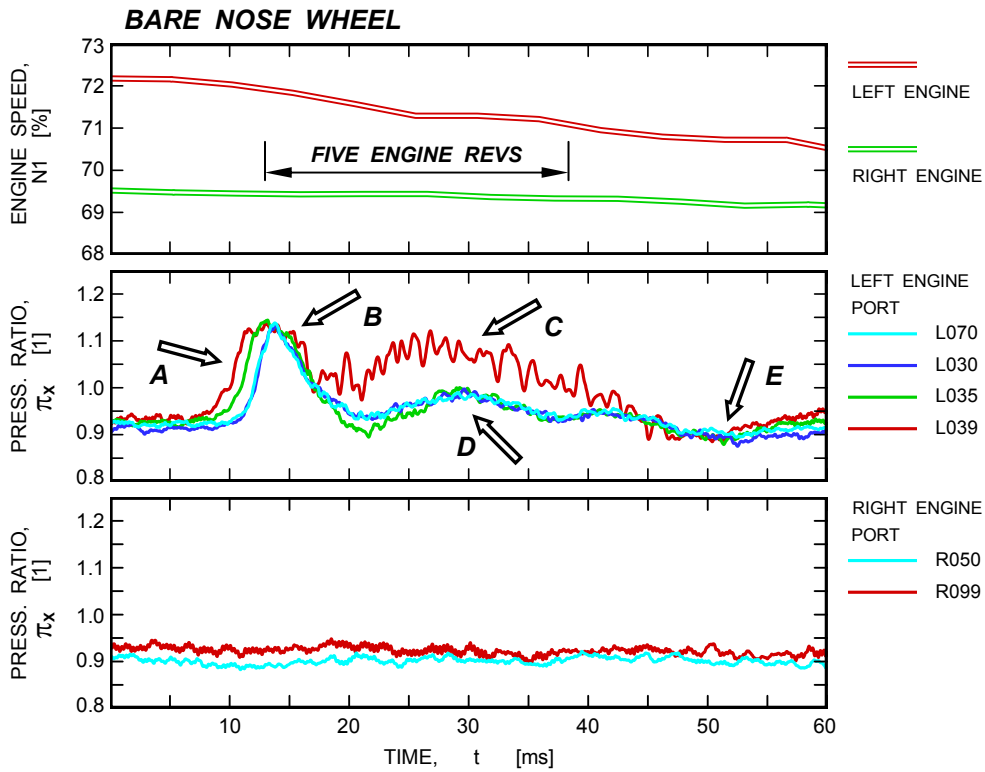


Fig. 6-5 Engine stall test *D1-04-18*; plotted time interval of 60 ms; filtered pressure data $f_{LP} = 1000$ Hz.

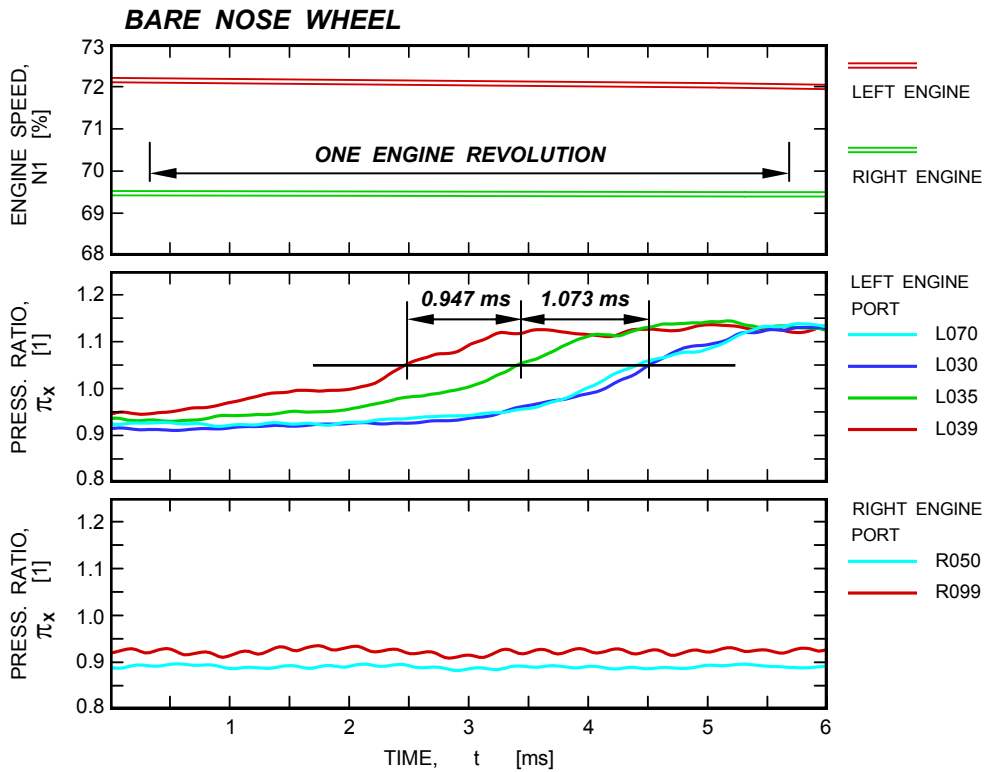


Fig. 6-6 Engine stall test *D1-04-18*; plotted time interval of 6 ms; filtered pressure data $f_{LP} = 1000$ Hz.

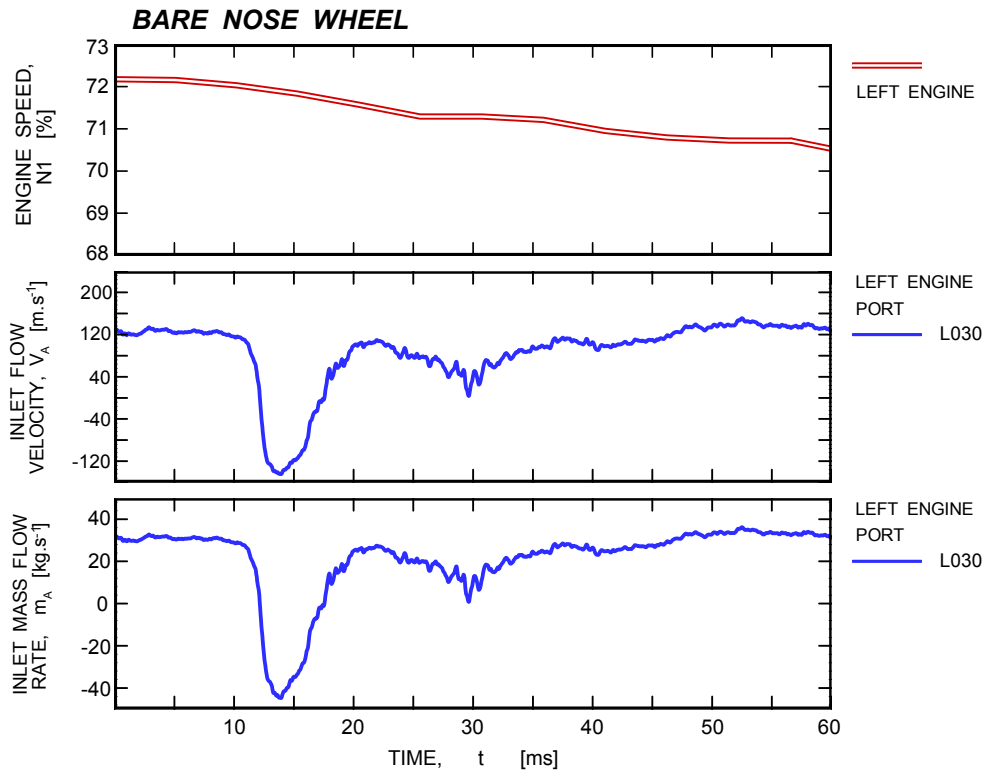


Fig. 6-7. Mass flow rate and inlet velocity variations during engine stall test D1-04-18; filtered data $f_{LP} = 1000$ Hz.

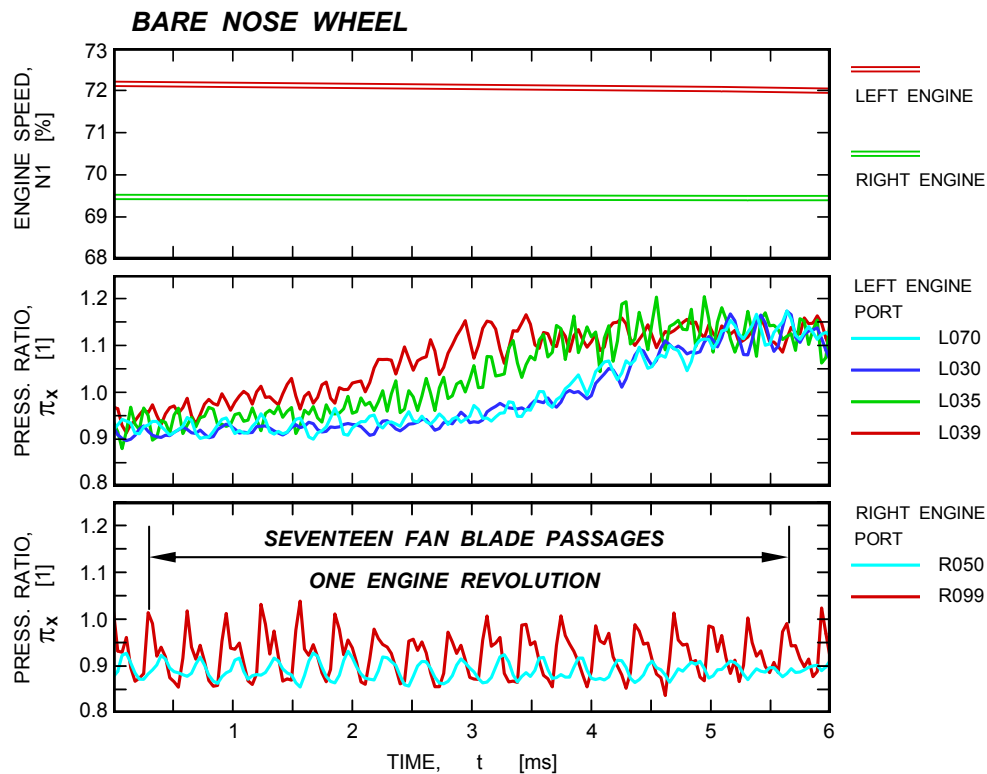


Fig. 6-8 Engine stall test D1-04-18; plotted time interval of 6 ms; unfiltered pressure data.

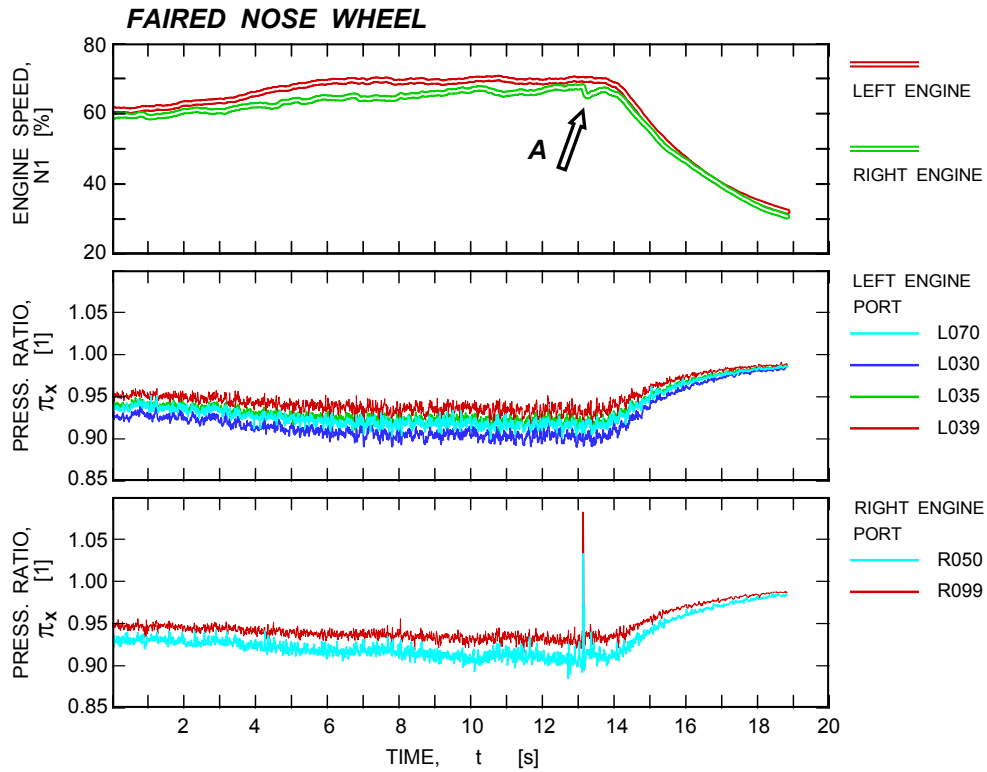


Fig. 6-9 Engine stall test *D1-04-07*; entire recorded segment of 18 s.

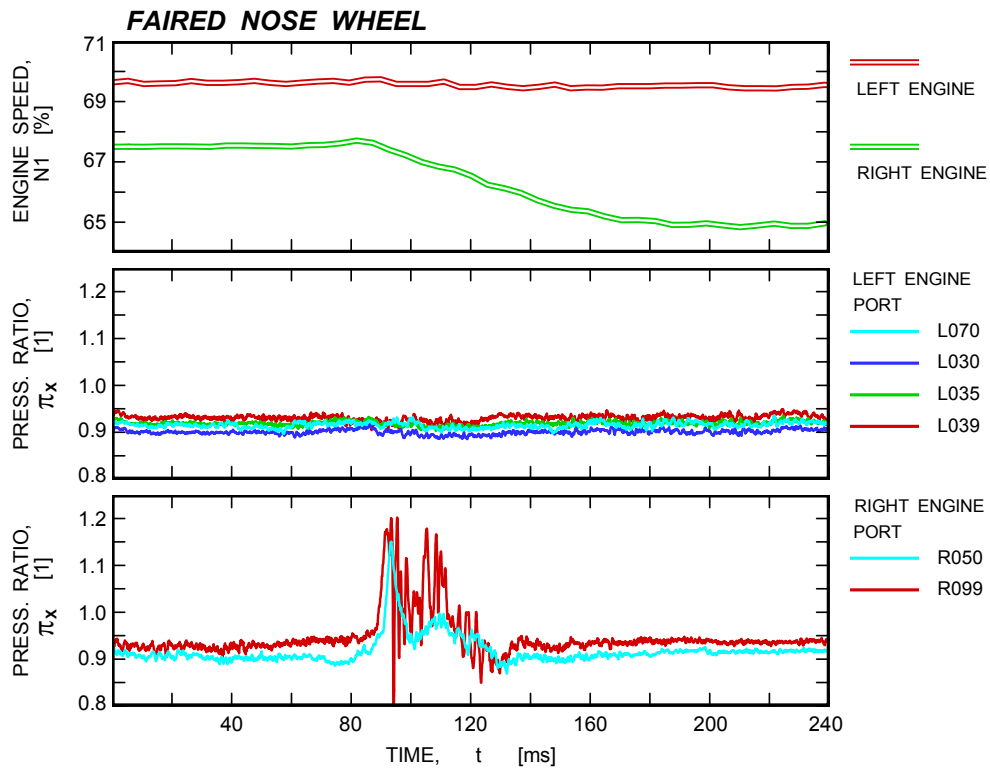


Fig. 6-10 Engine stall test *D1-04-07*; plotted time interval of 240 ms; filtered pressure data $f_{LP} = 1000$ Hz.

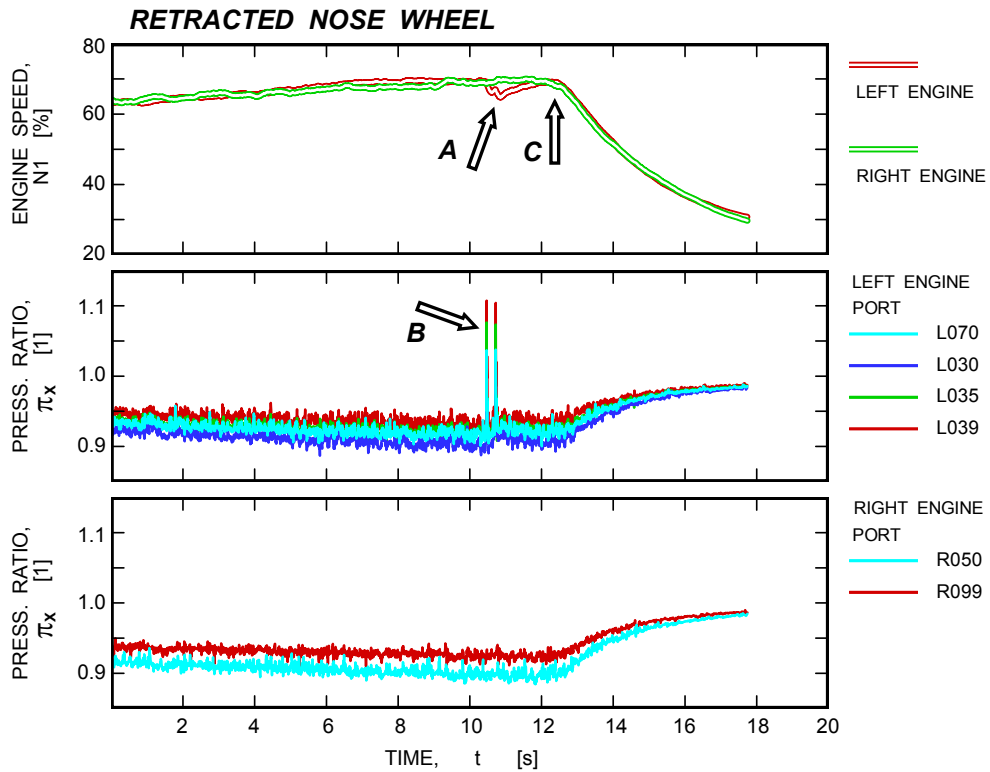


Fig. 6-11 Engine stall test *D1-03-18*; entire recorded segment of 18 s.

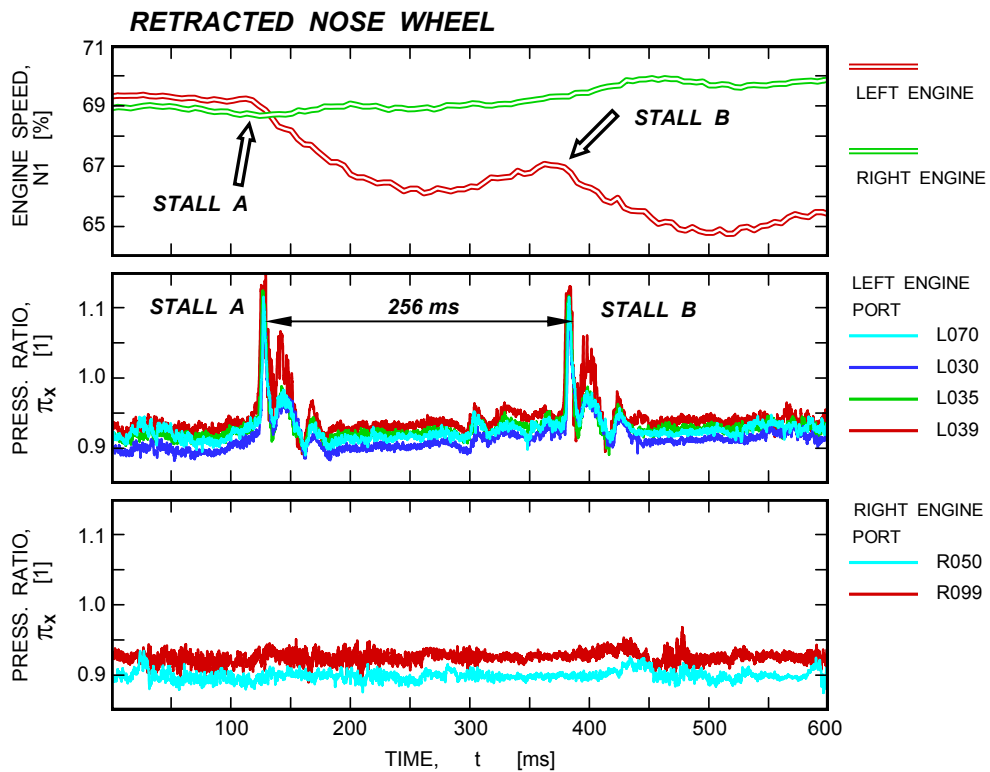


Fig. 6-12 Engine stall test *D1-03-18*; plotted time interval of 600 ms; unfiltered pressure data.

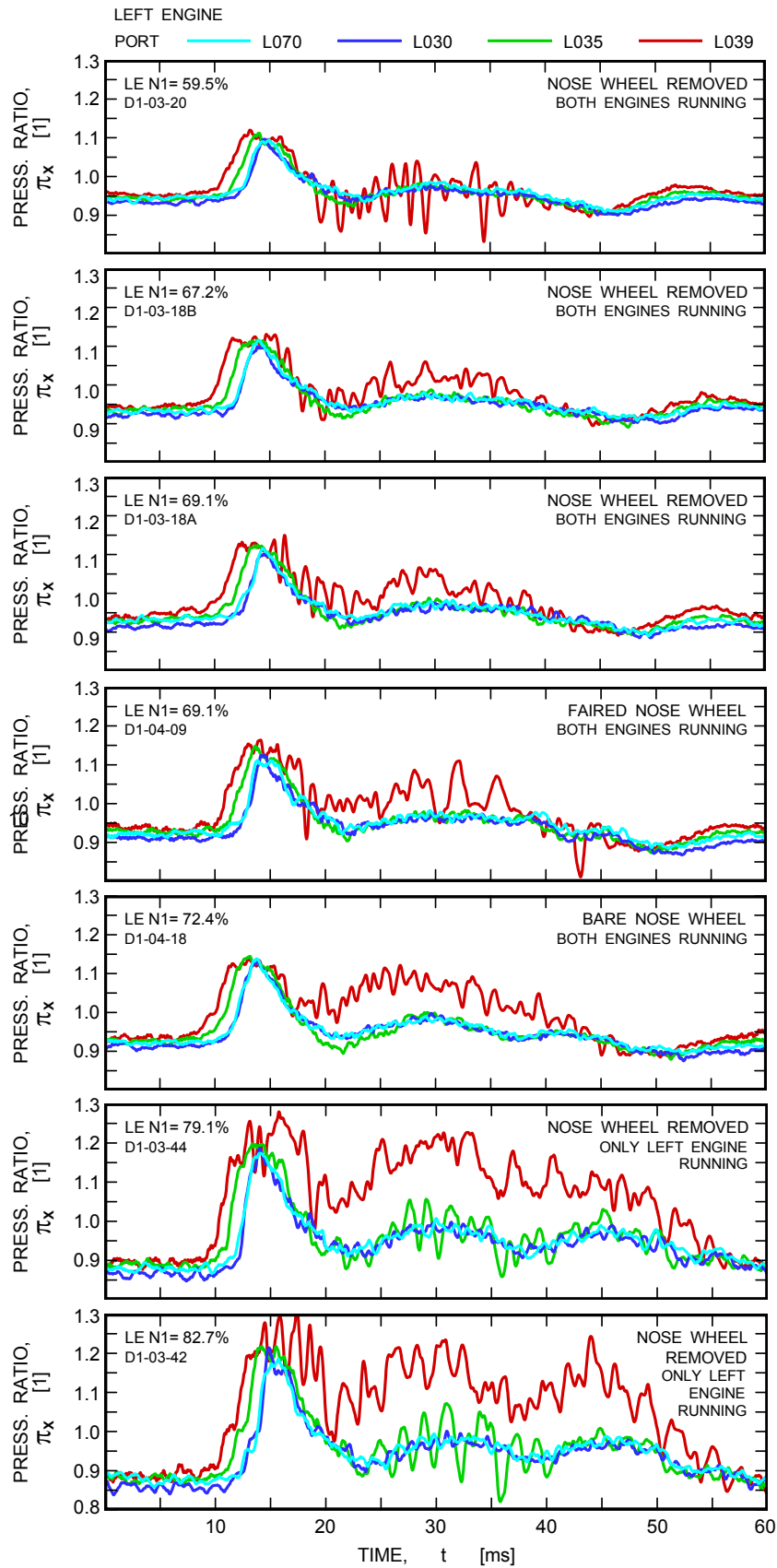


Fig. 7-1 Selected test conditions of left engine stalls.

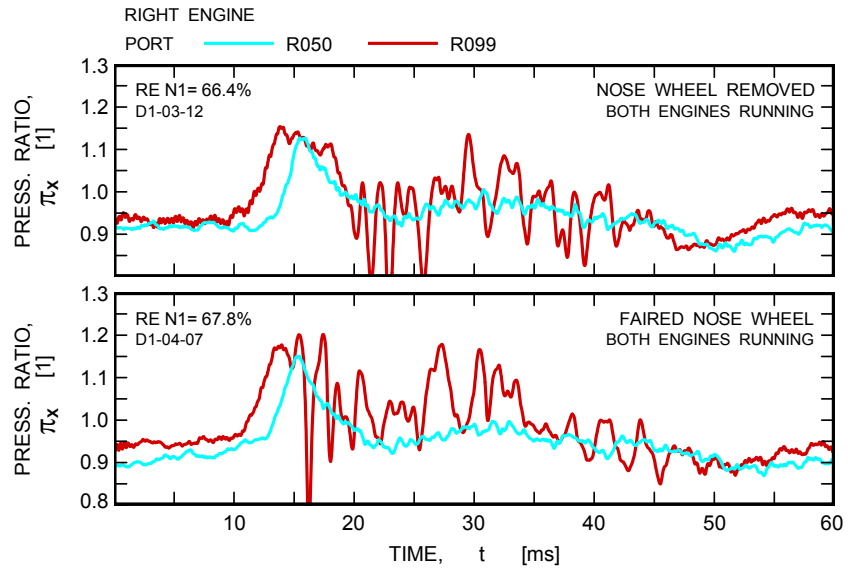


Fig. 7-2 Selected test conditions of right engine stalls.

REPORT DOCUMENTATION PAGE			Form Approved OMB No. 0704-0188		
<p>The public reporting burden for this collection of information is estimated to average 1 hour per response, including the time for reviewing instructions, searching existing data sources, gathering and maintaining the data needed, and completing and reviewing the collection of information. Send comments regarding this burden estimate or any other aspect of this collection of information, including suggestions for reducing this burden, to Department of Defense, Washington Headquarters Services, Directorate for Information Operations and Reports (0704-0188), 1215 Jefferson Davis Highway, Suite 1204, Arlington, VA 22202-4302. Respondents should be aware that notwithstanding any other provision of law, no person shall be subject to any penalty for failing to comply with a collection of information if it does not display a currently valid OMB control number.</p> <p>PLEASE DO NOT RETURN YOUR FORM TO THE ABOVE ADDRESS.</p>					
1. REPORT DATE (DD-MM-YYYY) 01-06-2008		2. REPORT TYPE Final Contractor Report		3. DATES COVERED (From - To)	
4. TITLE AND SUBTITLE Investigation of Flow Instabilities in the Inlet Ducts of DP-1C VTOL Aircraft			5a. CONTRACT NUMBER		
			5b. GRANT NUMBER NNCO6BA07B		
			5c. PROGRAM ELEMENT NUMBER		
6. AUTHOR(S) Lepicovsky, Jan			5d. PROJECT NUMBER		
			5e. TASK NUMBER		
			5f. WORK UNIT NUMBER WBS 561581.02.08.03.11.01		
7. PERFORMING ORGANIZATION NAME(S) AND ADDRESS(ES) ASRC Aerospace Corporation Cleveland, Ohio 44135			8. PERFORMING ORGANIZATION REPORT NUMBER E-16504		
9. SPONSORING/MONITORING AGENCY NAME(S) AND ADDRESS(ES) National Aeronautics and Space Administration Washington, DC 20546-0001			10. SPONSORING/MONITORS ACRONYM(S) NASA		
			11. SPONSORING/MONITORING REPORT NUMBER NASA/CR-2008-215216		
12. DISTRIBUTION/AVAILABILITY STATEMENT Unclassified-Unlimited Subject Category: 07 Available electronically at http://gltrs.grc.nasa.gov This publication is available from the NASA Center for AeroSpace Information, 301-621-0390					
13. SUPPLEMENTARY NOTES					
14. ABSTRACT An investigation of flow instabilities in the inlet ducts of a two-engine vertical takeoff and landing aircraft DP-1C is described in this report. Recent tests revealed that the engines stall during run ups while the aircraft is operating on the ground. These pop stalls occurred at relatively low power levels, sometimes as low as 60 percent of the engine full speed. Inability to run the engines up to the full speed level is attributed to in-ground effects associated with hot gas ingestion. Such pop stalls were never experienced when the aircraft was tested on a elevated grid platform, which ensured that the aircraft was operating in out-of-the-ground-effect conditions. Based on available information on problems experienced with other vertical takeoff and landing aircraft designs, it was assumed that the engine stalls were caused by partial ingestion of hot gases streaming forward from the main exit nozzle under the aircraft inlets, which are very close to the ground. It was also suggested that the nose wheel undercarriage, located between the inlets, may generate vortices or an unstable wake causing intense mixing of hot exit gases with incoming inlet flow, which would enhance the hot gas ingestion. After running a short three-day series of tests with fully instrumented engine inlets, it is now believed the most probable reason for engine pop stalls are random ingestions of a vortex generated between the two streams moving in opposite directions: outbound hot gas stream from the main nozzle close to the ground and inbound inlet flow above. Originally, the vortex is in a horizontal plane. However, at a certain velocity ratio of these two streams, the vortex attaches either to the ground or the aircraft surface at one end and the other end is swallowed by one of the aircraft inlets. Once the vortex enters the inlet duct, a puff of hot air can be sucked through the vortex core into the engine, which causes a serious inlet flow field distortion followed by an engine stall. Once the engine stalls, the outflow from the inlet pushes the vortex away and the engine resumes normal operation. This hypothesis needs to be verified experimentally; e.g., by extensive smoke flow visualization ahead of the aircraft inlets.					
15. SUBJECT TERMS Propulsion system performance instability engine test					
16. SECURITY CLASSIFICATION OF:			17. LIMITATION OF ABSTRACT	18. NUMBER OF PAGES 49	19a. NAME OF RESPONSIBLE PERSON STI Help Desk (email: help@sti.nasa.gov)
a. REPORT U	b. ABSTRACT U	c. THIS PAGE U			19b. TELEPHONE NUMBER (include area code) 301-621-0390

